TCC Training Seminar on
Seasonal Forecast

29 January – 2 February 2018

Tokyo, Japan

Tokyo Climate Center
Japan Meteorological Agency

TCC Training Seminar on Seasonal Forecast

29 January – 2 February 2018
Tokyo, Japan

Contents

Schedule
and
List of Participants

TCC Training Seminar on
Seasonal Forecast
Tokyo, Japan, 29 January - 2 February 2018

Schedule

Day 1 - Monday, 29 January		
10:00-10:30	1. Opening - Welcome Address - Self-introduction by participants - Group photo shooting - Courtesy call on JMA's Director-General	
10:30-10:45	Coffee Break	
10:45-11:00	2. Introduction: Outline and scope of the Training Seminar, and Introduction of the Tokyo Climate Center (TCC)	
11:00-12:30	3. Lecture: "Introduction to Climatology" for experts on climate services	
12:30-14:00	Lunch	
14:00-15:30	3. Lecture: "Introduction to Climatology" for experts on climate services	
15:30-15:45	Coffee Break	
15:45-16:15	4. Lecture: Introduction to reanalysis and JRA-55	
16:15-18:00	5. Exercise: Introduction and operation of iTacs (Basic)	
18:30-20:00	Reception	at KKR Hotel Tokyo
Day 2 - Tuesday, 30 January		
09:30-10:30	6. Lecture: Seasonal Forecast	
10:30-11:00	7. Lecture: Variability in the tropical oceans and its impact to the climate	
11:00-11:15	Coffee Break	
11:15-11:45	7. Lecture: Variability in the tropical oceans and its impact to the climate (cont.)	
11:45-12:45	8. Lecture: JMA's Ensemble Prediction System (EPS) for seasonal Forecasting	
12:45-14:15	Lunch	
14:15-16:45	9. Exercise: Introduction and operation of iTacs (Advanced)	
16:45-17:00	Coffee Break	
17:00-18:00	10. Lecture: Introduction of seasonal forecast guidance	
Day 3 - Wednesday, 31 January		
9:30-12:30	11. Exercise: Seasonal Forecast - Producing guidance and verification	
(Around 11:00)	Coffee Break	
12:30-14:00	Lunch	
14:00-17:00	11. Exercise: Seasonal Forecast (cont.) - Producing guidance and verification	
(Around 15:30)	Coffee Break	
17:00-18:00	12. Lecture: Interpretation of guidance, verification result and outputs from Numerical Prediction System (NWP)	
Day 4 - Thursday, 1 February		
9:30-12:30	13. Exercise: Generating seasonal forecast for your country - Preparation for presentation	
(Around 11:00)	Coffee Break	
12:30-14:00	Lunch	
14:00-15:00	13. Exercise: Generating seasonal forecast for your country (cont.) - Preparation for presentation	
15:00-18:00	14. Presentation by participants	Presentation (15 min.) followed by Q&A (5 min.)
(Around 16:00)	Coffee Break	
Day 5 - Friday, 2 February		
09:30-12:30	14. Presentation by participants (cont.)	
(Around 11:00)	Coffee Break	
12:30-12:50	15. Wrap up and Closing	
12:50-14:00	Lunch	
14:00-18:30	Technical Tour	

List of participants

Bangladesh
Mr Kh Hafizur Rahman
Meteorologist
Bangladesh Meteorological Department
Meteorological Complex, Agargaon, Dhaka-1207
Bangladesh
Tel: +88-029135742
Fax: +88-029119230
E-mail: rs77_hafizbmd@yahoo.com

Bhutan
Ms Pema Syldon
Hydro Meteorology Officer
Weather and Climate Services Division
National Center for Hydrology and Meteorology
Thimphu, Bhutan
Fax: +975-335578
E-mail: psyldon@nchm.gov.bt

Fiji
Mr Terry Atalifo
Principal Scientific Officer
Fiji Meteorological Service
Kororwai Road, NAP 0351, Nadi Airport
Fiji
Tel: +679-6724888
Fax: +679-6720430
E-mail: atalifo_terry@yahoo.com

Hong Kong, China
Mr Wing Hang Chan
Experimental Officer
Hong Kong Observatory
134A Nathan Road, Kowloon
Hong Kong, China
Tel: +852-2926-3104
Fax: +852-2375-2645
E-mail: whchan@hko.gov.hk

Indonesia
Mr Andhi Ahmad Setiawan
Staff of Climatology Station of Maros
The Agency for Meteorology, Climatology, and
Geophysics of Indonesia (BMKG)
Jl. Angkasa 1, No.2, Kemayoran, Jakartapusat
10610
Republic of Indonesia
Tel: +62-21-4246321
Fax: +62-21-6546336
E-mail: staklim.maros@bmkg.go.id

Lao People's Democratic Republic
Ms Akhom Thamalangsy
Officer
Department of Meteorology and Hydrology
Avenue Souphanouvong Avenue, Ban Akart
Village Sikhottabong District, P.O. Box 2903
Vientiane Capital
Lao People's Democratic Republic
Tel: +856 (21)215010 / +856 (020) 56225536
Fax: +856 (21) 223446
E-mail: akhomet@yahoo.com

Malaysia
Mr Mohamad Arif Bin Adenan
Assistant Director of National Weather Operation
and Geophysics Centre
Malaysian Meteorological Department
Jalan Sultan, 46667 Petaling Jaya, Selangor
Malaysia
Tel: +601-64332662
Fax: +603-79578052
E-mail: marif@met.gov.my

Mongolia
Mr Tsolmon Khishigsuren
Forecaster
Weather forecasting division
National Agency for Meteorology and
Environmental Monitoring (NAMEM)
15160 Juulchny gudamj-5, Ulaanbaatar
Mongolia
Tel: +976-90067010
Fax: +976-11-326611
E-mail: tsoomoo_1124@yahoo.com

Myanmar
Dr/Ms Soe Myat Mon
Staff Officer
Department of Meteorology and Hydrology
Room no (004), building no (a-2), YCDC staff estate, Hninsi Road, Yankin township, Yangon city
Myanmar
Tel: +95-9250068761
Fax: +95-01660524
E-mail: soemyatmon76@gmail.com

Nepal
Mr Subash Rimal
Meteorologist
Department of Hydrology and Meteorology
Nagpokhari, Naxal, Kathmandu
Nepal
Tel: +977-9849176116 / +977-01-4113191
Fax: +977-01-4473268
E-mail: rimalsubash@gmail.com

Pakistan
Mr Habib Rehmat
Meteorologist
Pakistan Meteorological Department
Institute of Meteorology & Geophysics, University Road, Karachi
Islamic Republic of Pakistan
Tel: +92-21-9926-1408
Fax: +92-21-9926-1405
E-mail: habib.rehmat@yahoo.com

Philippines
Ms Remedios L. Ciervo
Weather specialist II
Philippine Atmospheric, Geophysical and Astronomical Services Administration (PAGASA)
WFFC Bldg., Agham Road, Diliman, Quezon City
Republic of the Philippines
Tel: +63-2434-0955
Fax: +63-2434-0955
E-mail: remciervo@gmail.com

Mr Joseph Basconcillo
Weather specialist I
Philippine Atmospheric, Geophysical and Astronomical Services Administration (PAGASA)
Science Garden Complex, Agham Rd. Diliman, Quezon City
Republic of the Philippines
Tel: +63-2434-0955
Fax: +63-2434-0955
E-mail: jbasconcillo@pagasa.dost.gov.ph

Ms Rosemarie Ann A. Marasigan
Weather specialist I
Philippine Atmospheric, Geophysical and Astronomical Services Administration (PAGASA)
WFFC Bldg., Agham Road, Diliman, Quezon City
Republic of the Philippines
Tel: +63-2920-4076
Fax: +63-2920-4076
E-mail: raamarasigan@gmail.com

Singapore
Mr Wei Xiong How
Meteorologist
Meteorological Service Singapore
P.O. Box 8 Singapore Changi Airport, PTB II, South Finger, 918141
Singapore
Tel: 65-6542-5059
Fax: 65-6545-7192
E-mail: How_wei_xiong@nea.gov.sg

Solomon Islands
Mr Edward Maru
Senior Forecasting officer
Solomon Islands Meteorological Service Division
Solomon Islands Meteorological Services (SIMS)
P.O. Box 21, Honiara
Solomon Islands
Tel: +677-20332 / +677-24218 / +677-27658
Fax: +677-20332
E-mail: eddie.maru0@gmail.com

Sri Lanka
Ms Kariyawasam Ranaweera Kankanamalage
Dayani Nadeeka Ranaweera
Meteorologist
Department of Meteorology
383, Bauddhaloka Mawatha, Colombo 07
Sri Lanka
Tel: +94-075 7302003
Fax: +94-011 2698311
E-mail: ranaweerakrkdn@yahoo.com

Thailand
Mr Chaowat Siwapornchai
Meteorologist
Thai Meteorological Department
4353 Sukhumvit Road, Bangna,
Bangkok 10260
Kingdom of Thailand
Tel: +66-23989929 / +66-838269823
Fax: +66-23838827
E-mail: sam.cwsp@gmail.com,

Viet Nam
Ms Thi Anh Dang
Forecaster
Red River Delta Regional Hydro-Meteorological Center, National Hydro-Meteorological Service of Vietnam
No 62/2 Nguyen Chi Thanh Street, Dong Da, Ha Noi
Vietnam
Tel: +84-43 77 3 1309
Fax: +84-43 77 3 1309
E-mail: phuonganhdbkt@gmail.com

“Introduction to Climatology”
for experts on climate services

“Introduction to Climatology” for experts on seasonal forecasting

Ryo MIZUTA (rmizuta@mri-jma.go.jp)
Climate Research Department, Meteorological Research Institute (MRI/JMA)
1-1 Nagamine, Tsukuba, 305-0052, JAPAN

1. Climate and Climate system

According to WMO website, “on the simplest level the weather is what is happening to the atmosphere at any given time. Climate, in a narrow sense, can be considered as the ‘average weather,’ or in a more scientifically accurate way, it can be defined as ‘the statistical description in terms of the mean and variability of relevant quantities over a period of time.’” Although climate is the synthesis of the weather, climate is not maintained only by atmosphere itself but is formed in the interactions among many components of the Earth. This system is named as a climate system. The global climate system consists of atmosphere including its composition and circulation, the ocean, hydrosphere, land surface, biosphere, snow and ice, solar and volcanic activities (Fig.1). These components interact on various spatial and temporal scales through the exchanges of heat, momentum, radiation, water and other materials.

The purpose of the lecture is to know how climate is formed and its variability is caused. In the lecture, anthropogenic “climate change” defined by United Nations Framework Convention on Climate Change (UNFCCC) is also included.

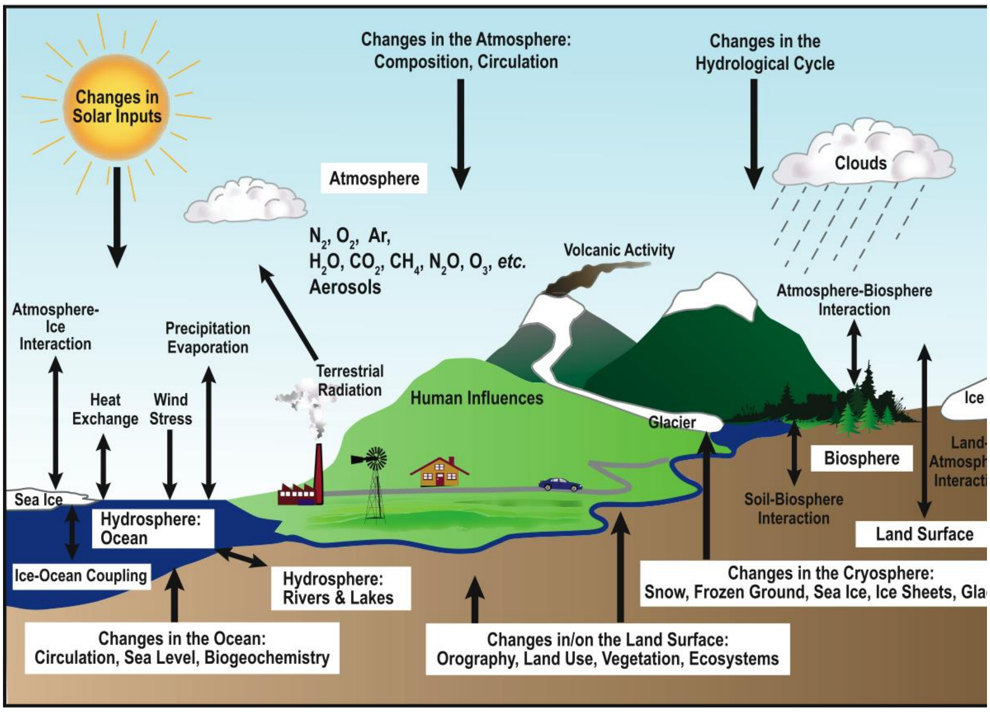

Figure 1 Schematic view of the components of the climate system, there processes and interactions. From IPCC (2007).

2. Global mean temperature and Radiative balance

Global mean temperature of planets, which is the temperature “observed from space”, is estimated by global radiation balance between absorbed solar radiation and terrestrial emission from the planet. Incoming solar radiation is reflected back to space by a fraction of the planetary albedo. For the Earth, the observed mean ground temperature (15°C) is warmer by 34°C than the estimated temperature (-19°C). The reason is suggested by comparing other planet cases. The mean ground temperature for Mars with thin atmosphere is warmer only by 1°C than the estimated temperature. For Venus with thick atmosphere, the difference is 503°C. Radiative absorption by greenhouse gas in atmosphere is an important factor to determine mean ground temperature as well as planetary albedo.

The Earth’s atmosphere has different characteristics for shortwave and longwave radiations (Fig.2). It is transparent (about 50%) for shortwave radiative flux from the sun as an approximation except for the reflection due to clouds (about 20%). On the other hand, the longwave radiation flux emitted from the Earth’s ground is absorbed (about 90%) once in the atmosphere approximately and then mostly emitted back to the ground (greenhouse effect). Upper cold atmosphere and clouds emit less longwave flux to space than the ground emits. As a net, surface ground is heated by shortwave radiation from the sun, and atmosphere is cooled by longwave emission to space. The vertical contrast of the heating between ground and atmosphere creates thermal instability, which is compensated by vertical transport processes of sensible and latent heat energy due to turbulences, convections and waves.

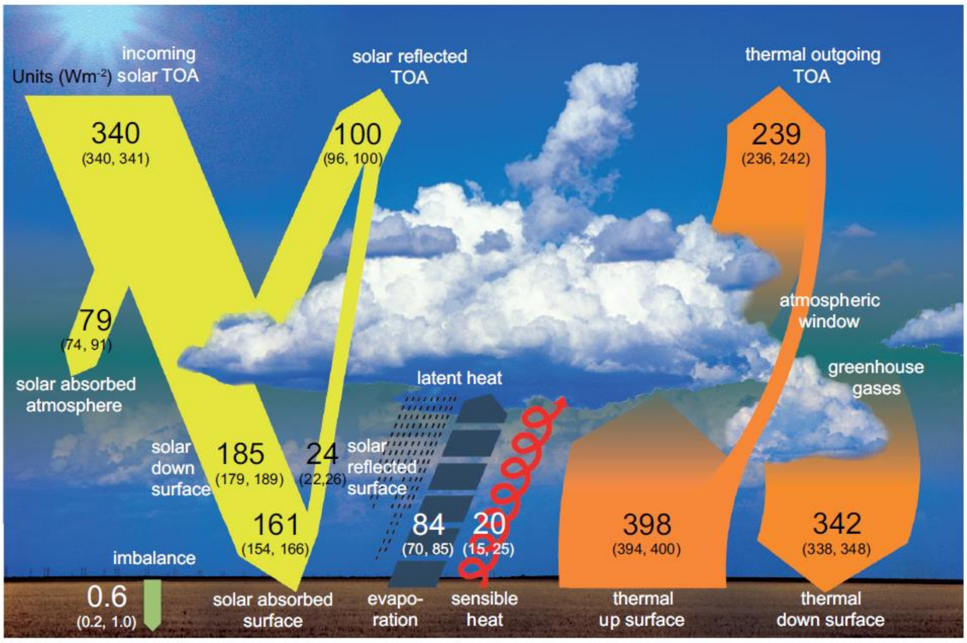

Figure 2 Schematic diagram of the global mean energy balance of the Earth. Numbers indicate best estimates for the magnitudes of the globally averaged energy balance components together with their uncertainty ranges, representing present day climate conditions at the beginning of the twenty first century. Units W/m^2. From IPCC (2014).

3. Annual mean circulation and Horizontal heating contrast

Longitudinal contrast of radiative heating is created between day and night (Fig.3). But, generally, as compared with the annual cycle, the diurnal heating contrast does not produce significant temperature differences between day and night and related global circulations because a relaxation time to a radiative equilibrium is estimated as 30 days for the Earth (James, 1995), which is much longer than a day scale. Latitudinal heating contrast on the Earth is created on seasonal time-scale by the different incoming shortwave radiation between near the poles and the tropics (Fig.3). Local surface temperature determining outgoing longwave radiation is not adjusted instantly enough to compensate for the shortwave radiation contrast. A part of absorbed radiative energy in low latitudes is transported poleward by meridional circulations and waves in atmosphere and ocean, and these heat transports keep high-latitudes warmer than the radiative equilibrium.

Poleward/equatorward air motions form westerly/easterly wind in the upper/lower subtropics (Fig.4) through Coriolis force due to the rotation of the Earth (or the angular momentum conservation about the Earth's rotation axis). Extra-tropical waves are also responsible for creating mid- to high latitude's westerly jets.

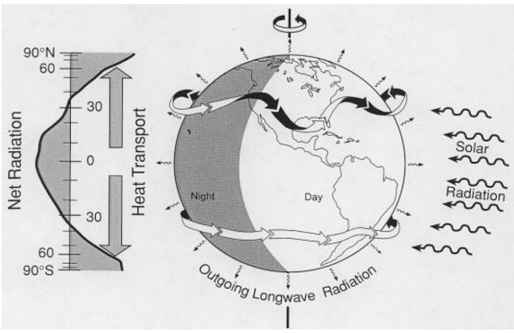

Figure 3 Horizontal radiative imbalance and energy transport by the atmosphere and ocean. From IPCC (1995).

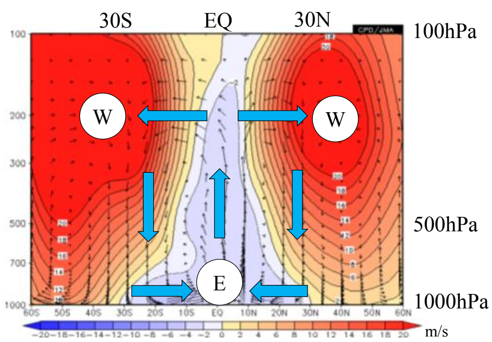

Figure 4 Annual and zonal mean wind. Shade: zonal wind, and arrow: meridional and vertical wind.

4. Seasonal change and Heat capacity

Seasonal change is definitely produced by the seasonally changing solar incidence with its maxima at the South Pole in December and at the North Pole in June. However, zonally averaged features of temperature are not drastically changed in the troposphere (lower than about 100hPa) through the whole year, hot tropics and cold poles (Fig.5). This fact is attributed to basically unchanged distribution of sea surface temperature (SST) due to large heat capacity of the oceans; in the Earth, heat capacity of the ocean is about 1,000 times of that of the atmosphere. SSTs roughly determine the location of deep cumulus occurrences, which leads to vertical energy mixing in the troposphere and drives global circulations (Webster, 1994). Stratospheric climate above 100hPa varies following the seasonal march of the sun (Fig.5) because of the seasonal change of ozone-related shortwave heating and small heat capacity of thin stratospheric atmosphere; cold around a winter pole, warm around a summer pole. Atmospheric circulations also contribute to the stratospheric climate; a cold tropopause in the tropics is steadily created by upward motion.

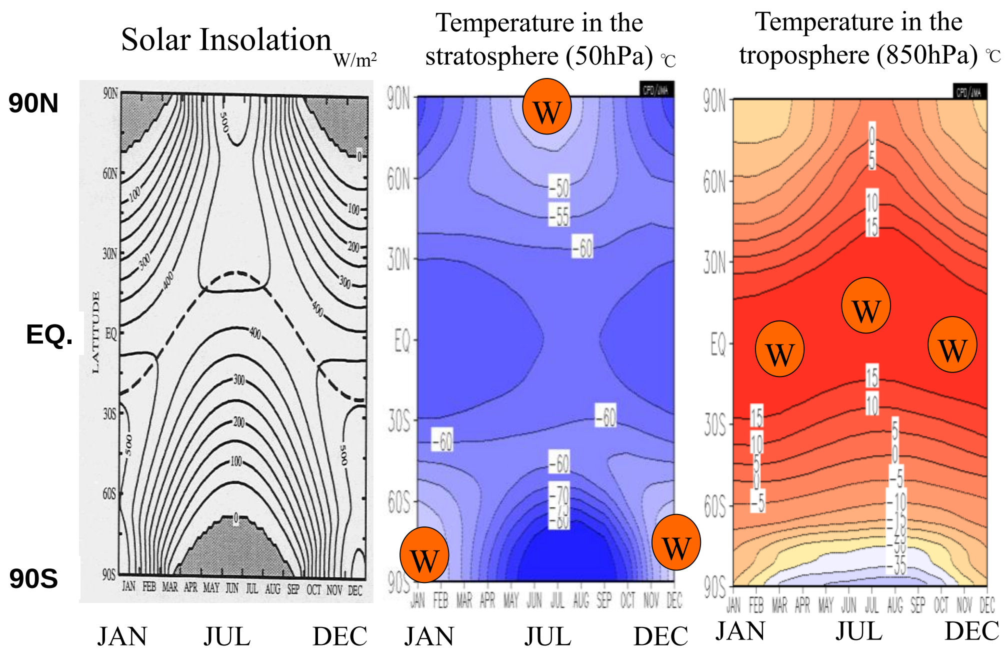

Figue 5 Seasonal change of (left)solar insolation, zonally averaged temperature (middle) at 50hPa and (right) at 850hPa. The figure for solar insolation is from IPCC (1995).

Heat capacity of land surface is small as compared with that of the oceans. Surface air temperature over the northern continents is much higher than SSTs at the same latitudes in the northern summer (especially in daytime) and much colder in the northern winter (Fig.6). The large contrasts of surface air temperature between continents and the oceans add a significant feature to regional seasonal changes of rainfall and wind around the continents in low and mid-latitudes, which is named as monsoon. A concentrated subtropical rainfall forms a typical summer monsoon system consisting of an upper-level anti-cyclonic circulation, a monsoon trough, a low-level jet, a subtropical rainfall band expanding north eastward (south eastward) and extensive downward motions causing dry region in the north westward (south westward) area of the Northern (Southern) Hemisphere (Rodwell and Hoskins, 1996), as shown in the Asian region of Fig.6 and Fig. 7.

Jan-Jul contrast of surface temperature/precipitation

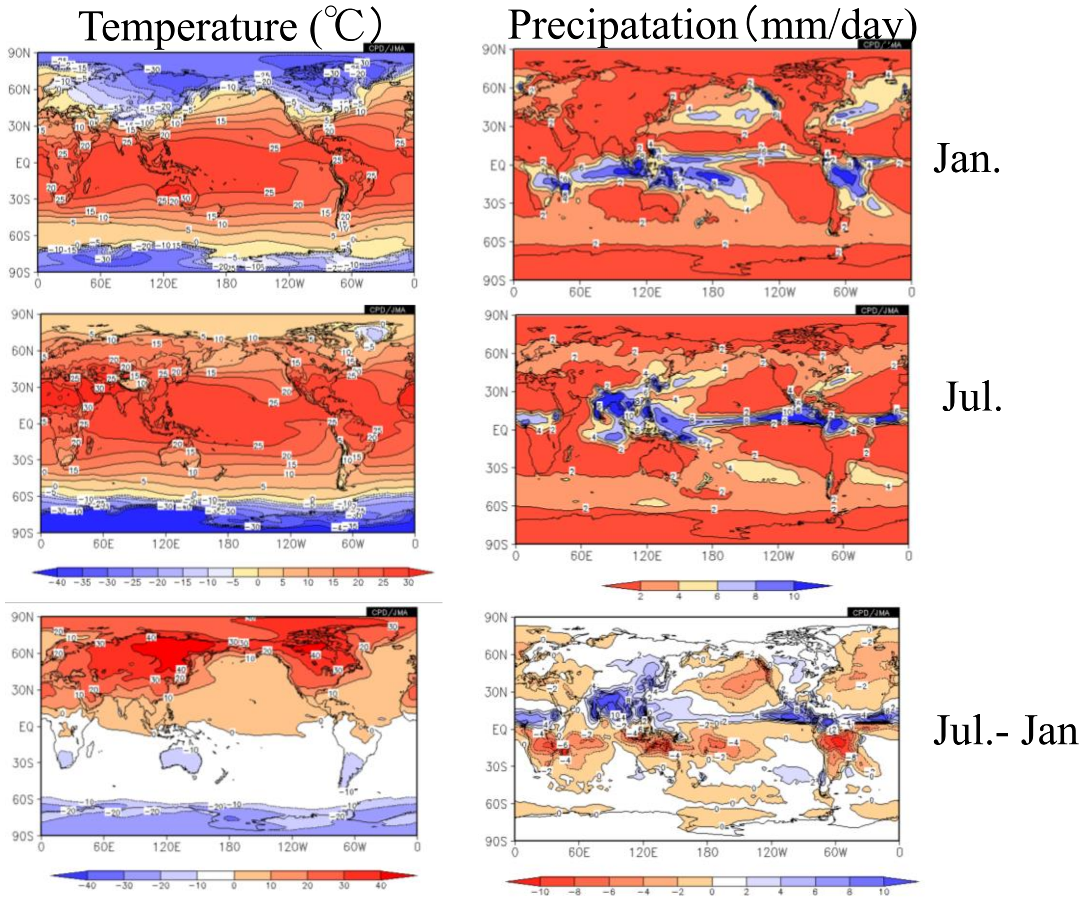

Figure 6 (Left) surface are temperature and (right) precipitation in (upper) January, (middle) July, and (bottom) deference between the two months.

Northern Summer Monsoon circulation

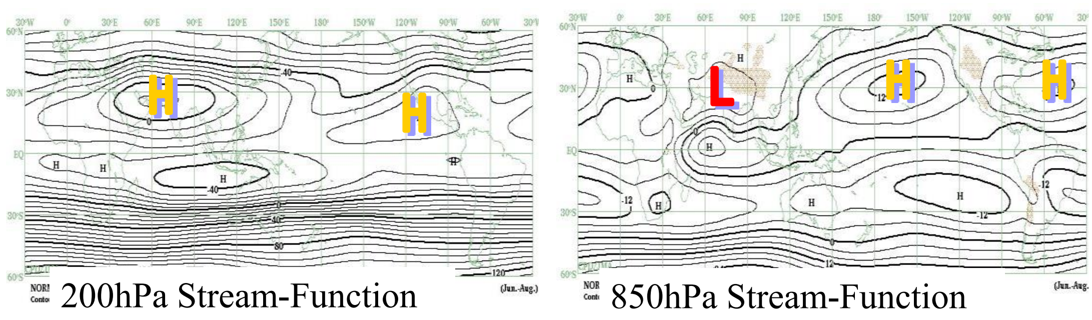

Figure 7 (Left) 200hPa stream function and (right) 850hPa stream function in JJA.

Mountains have also impact on seasonal changes in local climate through thermal and dynamical processes. A good way to understand climate system is to modify or remove some elements of the climate system (Fig. 1). It is not easy to modify a real climate system of the Earth by changing the Earth orbit or removing mountains. Instead, we can easily modify virtual climate systems simulated numerically in climate models based on physics and other fundamental sciences. From the comparison between with/without mountain model experiments (Fig. 8), we can see that mountains would be responsible for the real world climate of humid summer and somewhat cold winter in the eastern parts of the continents.

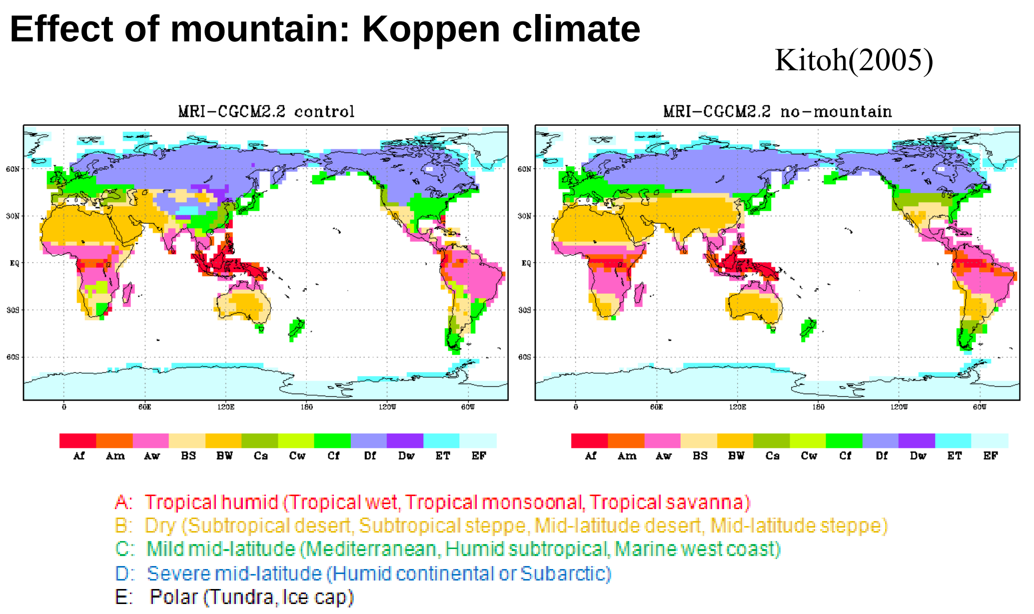

Figure 8 Koppen climate maps simulated by a climate model (left) with mountains and (right) without mountains. From Kitoh (2005) in Japanese.

6. Intra-seasonal to Interannual variability

Climate varies naturally with time. Atmosphere itself includes internal instability mechanisms, typically the baroclinic instability around the extratropical westerly jets, so that it may be considered as chaotic or unpredictable beyond a few weeks. However, some atmospheric low-frequency (>10days) teleconnections are analyzed such as wave patterns along the westerly jet waveguides and other ones from the northern mid-latitudes across the equatorial westerlies (Fig. 9), which are consistent with the Rossby-wave propagation theory. Also, teleconnections of another type are analyzed such as meridional displacements of the westerly jet (Fig.10), which are maintained by the wave-mean flow interaction (Vallis, 2006). Numerical ensemble predictions from many disturbed atmospheric initials are a reasonable tool to capture mean weathers in next few weeks.

Teleconnection and Rossby-wave propagation

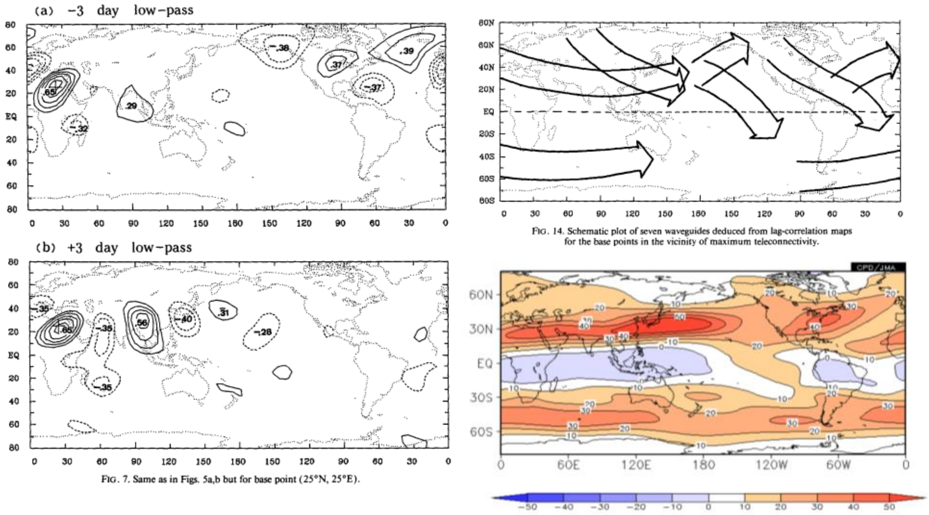

Figure 9 (Left) a teleconnection pattern of 250hPa stream function in boreal winter, (upper-right) various propagations of Rossby-wave and (lower-right) 250hPa climatological zonal wind in DJF. Left and upper-right panels are from Hsu and Lin (1992).

North Atlantic Oscillation (NAO)

Positive phase　　Negative phase

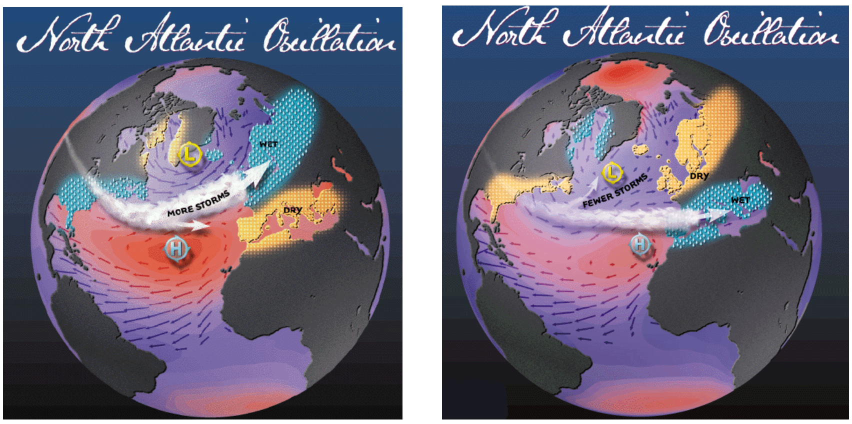

From http://www.ldeo.columbia.edu

Figure 10 (Left) positive and (right) negative phase of North Atlantic Oscillation (NAO). NAO is one of teleconnections with meridional displacements of the westerly jet. Panels are from http//www.ldeo.columbia.edu.

In the tropics, some peaks in spatial and temporal power-spectrums, indicating organized atmospheric variability coupled with convective activity, are imbedded in red noise backgrounds. Variability of outgoing longwave radiation (OLR) associated with equatorial waves, such as Kelvin waves, equatorial Rossby waves (ER) and mixed Rossby-Gravity waves (MRG), can be detected, in Fig. 11.

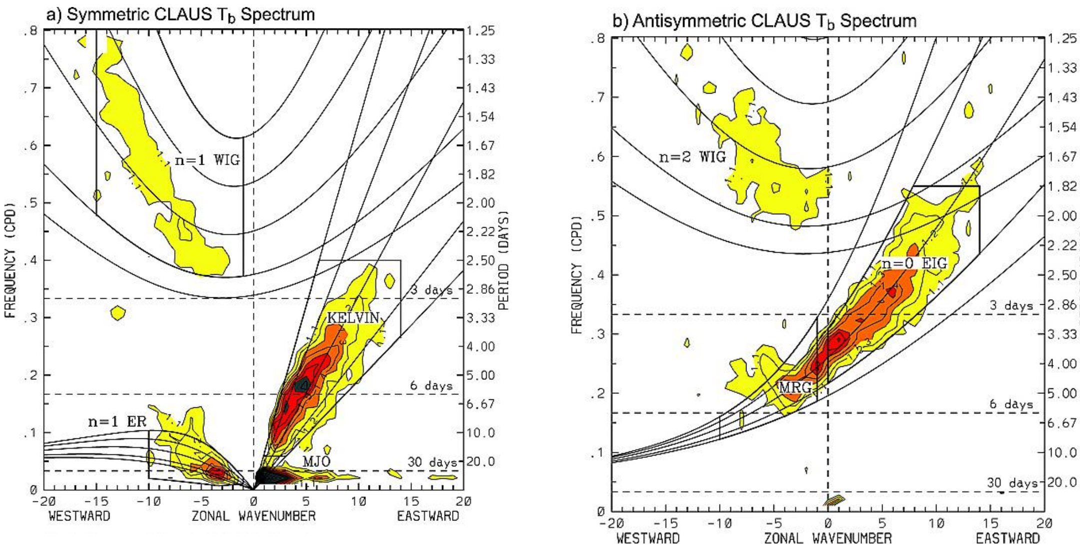

Wave number–frequency power spectrum of the (a) symmetric and (b) antisymmetric component of Cloud Archive User Services (CLAUS) T_b for July 1983 to June 2005, summed from 15° N to 15° S, plotted as the ratio between raw T_b power and the power in a smoothed red noise background spectrum (see WK99 for details). Contour interval is 0.1, and contours and shading begin at 1.1, where the signal is significant at greater than the 95% level. Dispersion curves for the Kelvin, *n* = 1 equatorial Rossby (ER), *n* = 1 and *n* = 2 westward inertio-gravity (WIG), *n* = 0 eastward inertio-gravity (EIG), and mixed Rossby-gravity (MRG) waves are plotted for equivalent depths of 8, 12, 25, 50, and 90 m. Heavy solid boxes represents regions of wave number–frequency filtering

Figure 11 Spatial and temporal power-spectrums in the tropics of (left) symmetric and (right) asymmetric OLR variability about the equator. (From Kiladis et al. 2009).

The Madden-Julian Oscillation (MJO) is an eastward-moving oscillation of surface pressure, precipitation and winds along the equator with the period of 30-60 days and planetary scale wavenumbers (Fig. 12). Monitoring MJO or watching OLR and velocity potential anomalies may be very helpful for intra-seasonal prediction in the tropics to the subtropics and even in the mid-latitudes (Fig. 12). Improvement of MJO prediction skill is one of key topics for operational numerical prediction centers in the world.

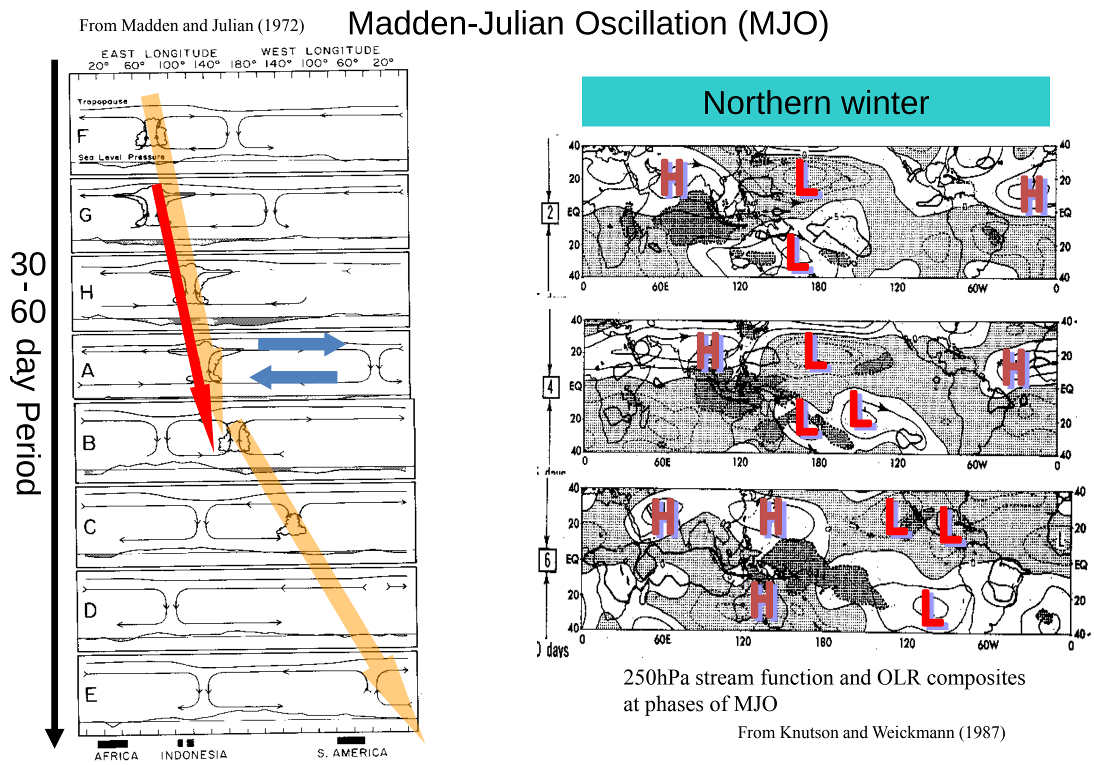

Figure 12 (Left) schematic time-sequence of Madden-Julian Oscillation (MJO) along the equator (from Madden and Julian, 1972). (Right) composite maps of OLR and 250hPa stream function anomaly at MJO phases (from Knutson and Weickmann 1987).

Atmosphere-ocean interactions are able to produce longer time-scale natural variability in atmosphere with periods beyond months up to several and decadal years. A typical example is ENSO (El Niño / Southern Oscillation) with the period of 2-7 years, which is the most dominant interannual climate variability in the earth climate system and has huge sociological and economic impacts globally. El Niño events themselves, and related surface air temperature and precipitation anomalies are predicted successfully on seasonal to inter-annual scales (Fig.13). The SST anomalies with El Niño tend to keep seasonally steady precipitation (heating) anomalies over the equatorial central Pacific. The response of the upper and lower-level tropical atmosphere to these steady heating anomalies can be explained based on forced equatorial waves or the Gill-pattern (or Matsuno-Gill pattern) (Fig. 14). These anomalous steady heating in the tropics forces stationary Rossby waves which propagate to mid-latitudes, and tends to cause teleconnection patterns such as the Pacific North America (PNA) pattern and the Western Pacific (WP) pattern.

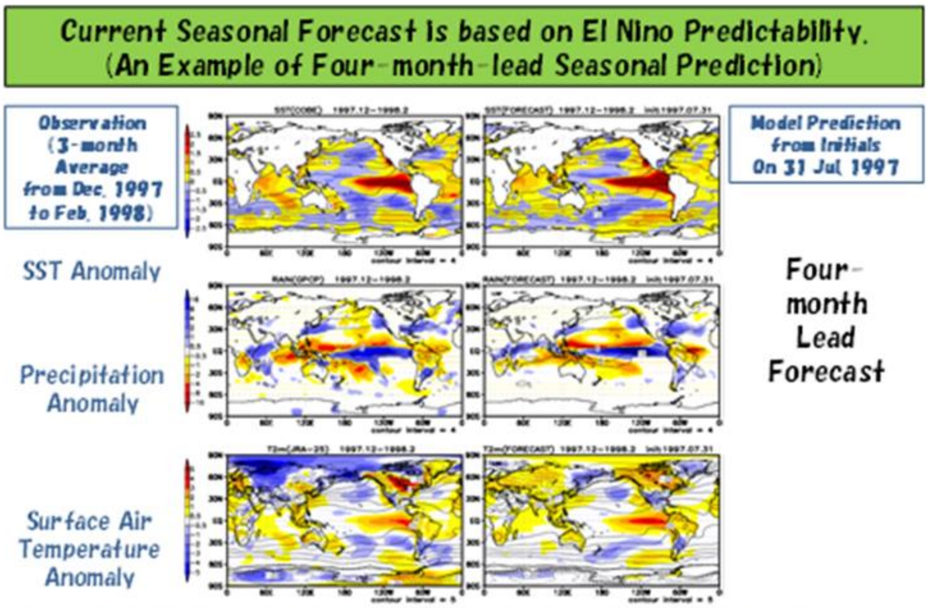

Figure 13 (Left) observed SST, precipitation and surface air temperature anomalies for DJF 1997-98. (Right) the same except for four-month lead prediction.

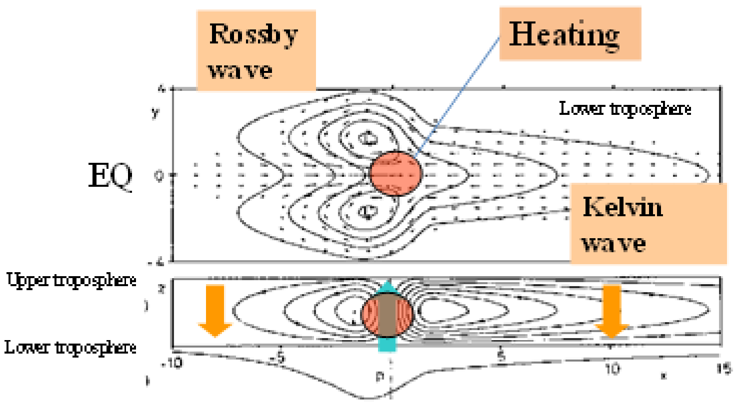

Figure 14 Tropical atmospheric responses to equatorially symmetric heating anomalies. (from Gill 1980).

Recently, terms of “El Niño Modoki” or “Central Pacific (CP)-El Niño” are used to distinguish them from normal El Niño events or Eastern Pacific (EP)-El Niño. They consist of the equatorial Pacific phenomena with warm SST anomalies and enhanced precipitation in the central Pacific, and cold SST anomalies and suppressed precipitation in the eastern Pacific, on contrast. The remote effect of El Niño during the mature stage is stored in the Indian Ocean capacity and still influential to the Indo-western Pacific climate even during summer following the ENSO (Fig.15). A dipole mode with an east-west SST anomaly contrast sometimes occurs around September and October in the tropical Indian Ocean, which is at least partially independent from ENSO events (Fig. 16). Occurrence of this mode affects climate over various regions including tropical eastern Africa and the maritime continent.

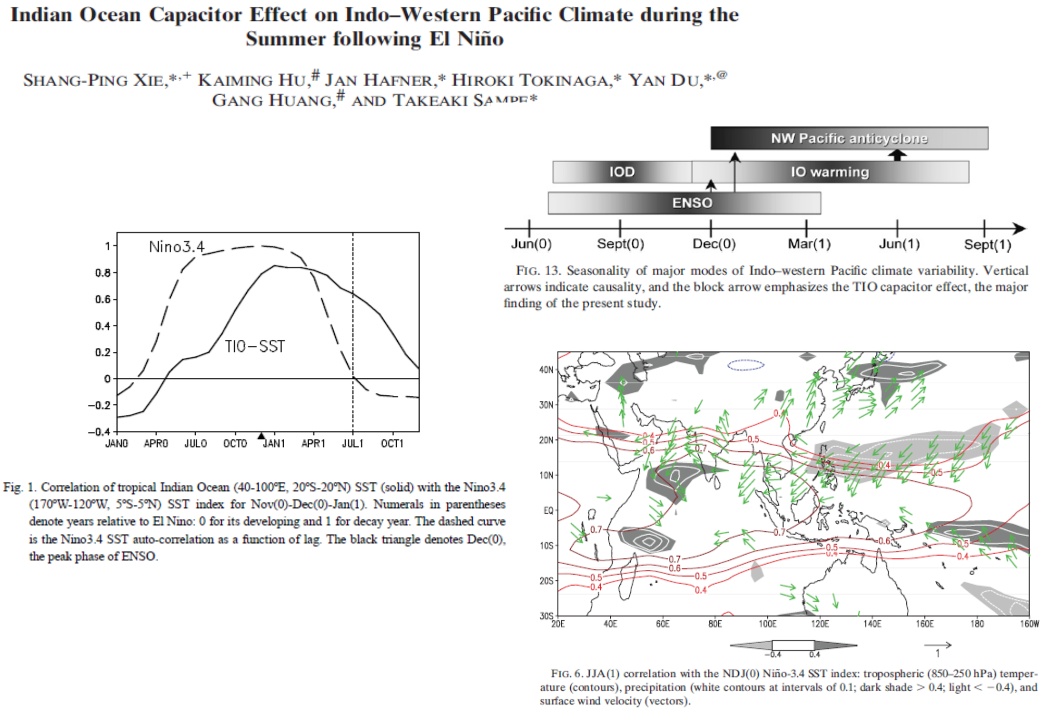

Figure 15 Indian Ocean capacitor effect. (Left) lagged correlation of tropical Indian Ocean SST with Nino 3.4 SST for NDJ. (Upper-right) seasonality of major modes. (Lower-right) correlation of the NDJ Nino3.4 SST with the following JJA climate. From Xie et al. (2009).

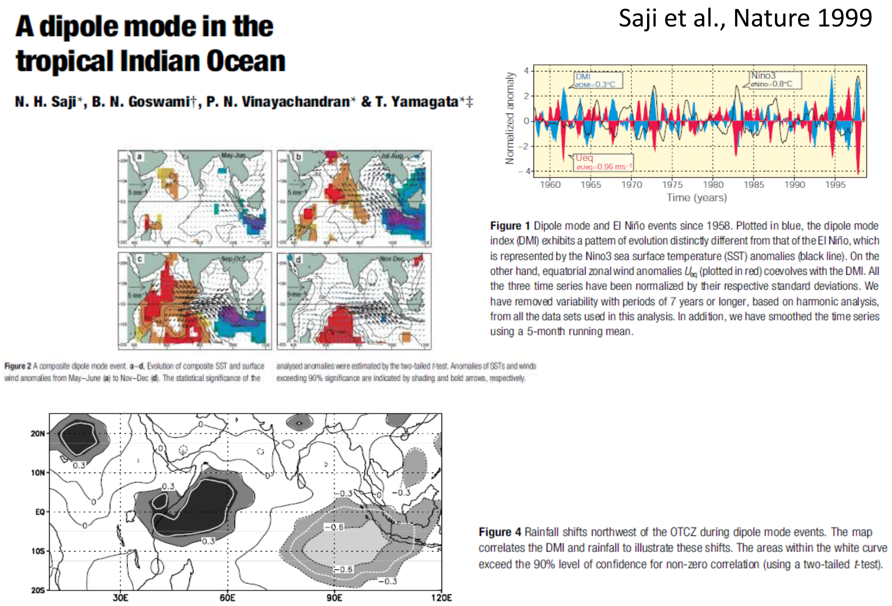

Figure 16 A dipole mode in the tropical Indian Ocean. (Upper-left) time-evolution of the dipole

7. Decadal variability

Decadal variability and climate change involve feedbacks from other elements of the climate system. Changes of vegetation and soil moisture amplify the dramatic drying trend in 1980's in Sahel region, which is basically forced by a southward precipitation shift of the Inter-tropical Convergence Zone due to cooler/warmer SST anomaly in the northern/southern Atlantic Ocean (Fig. 17).

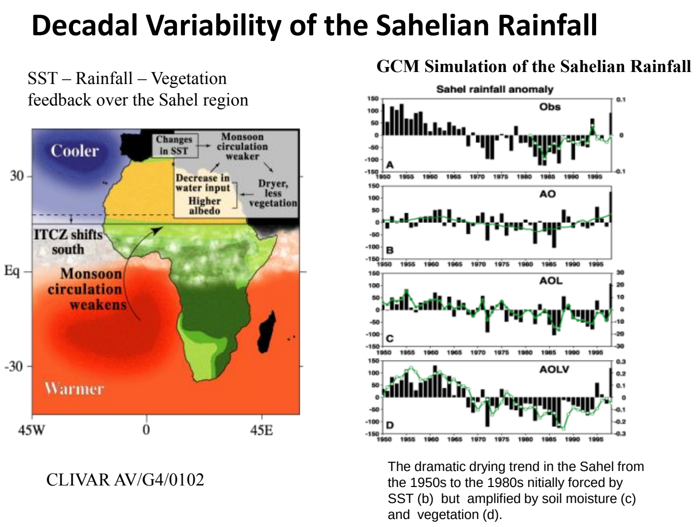

Figure 17 Decadal variability of the Sahel Rainfall. (Left) a possible mechanism, (Right) observed historical Sahel rainfall anomaly and GCM simulations . From Zeng et al. 1999.

Decadal variabilities are also found in SST anomaly from the North Pacific to the tropics (Fig. 18) which is named Pacific Decadal Oscillation (PDO) or Interdecadal Pacific Oscillation (IPO). A possible mechanism of PDO is the subduction hypothesis; high latitudes' cold surface water is subducted in the North Pacific and flows into the subtropical deeper ocean along the surfaces of constant density, then emerges again to the surface of the equatorial Pacific by upwelling. This is consistent with the analysis showing that the decadal SST variability in the central North Pacific spreads into the deep ocean. PDO has impact on ENSO characteristics and regional climate. Several studies indicated that the negative phase of PDO played the major role in the slowdown of the global averaged surface air temperature raise in recent years (Meehl, 2015).

Pacific Decadal Oscillation

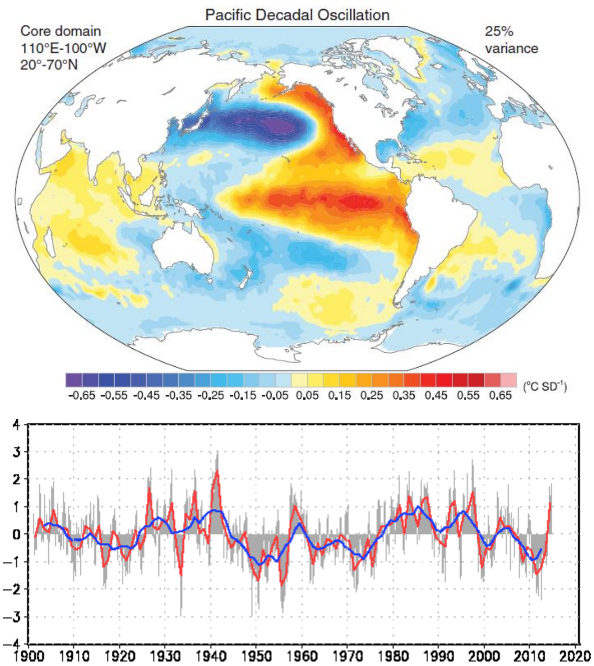

Trenberth and Fasullo (2013)

PDO index (From JMA HP)

Figure 18 (Upper) SST anomaly pattern in the positive phase of Pacific Decadal Oscillation (PDO)(from Trenberth and Fasullo, 2013) and (lower) PDO index (from http://ds.data.jma.go.jp/tcc/tcc/products/elnino/decadal/pdo.html).

8. Summary

Unusual weather and climate are attributed to unusual atmospheric flows, storms and convective disturbance. Diagnostic analysis shows that those disturbances are often related to atmospheric intrinsic waves and phenomena. However, atmospheric environment is maintained and influenced by other elements consisting of the climate system. Sometimes, and unusual and steady convective activity is connected to long-term SST anomalies related to ocean variability. Numerical ensemble simulations starting from many disturbed atmospheric and oceanic initials are a reasonable tool to capture the mean state of weathers and climate in a timescale from weeks to seasons. Radiative processes including longwave absorption by greenhouse gases and shortwave reflection by snow, ice, clouds and aerosols determine the local Earth's ground temperature. The distribution of ground temperature is influential to vertical and horizontal atmospheric and oceanic stabilities, the amount of water vapor and the speed of water cycle. Then, those can affect atmospheric and oceanic flows, the features of storms and convections and eventually our daily lives. Therefore, we need to continue careful watches and diagnostics for global and local climate systems (Fig.1), as well as its prediction.

References

Deser, C., M. A. Alexander and M. S. Timlin, 1996: Upper-ocean thermal variations in the North Pacific during 1970-1991. *J. Climate*, **9**, 1840-1855.

Gill, A. E., 1980: Some simple solutions for heat-induced tropical circulation. *Quart. J. Meteor. Soc.*,**106**, 447-462.

Hsu, H.-H., and S.-H. Lin, 1992: Global teleconnections in the 250-mb streamfunction field during the Northern Hemisphere winter. *Mon. Wea. Rev.*, **120**, 1169-1190.

IPCC Second Assessment Report (SAR) Climate Change 1995: The Science of Climate Change.

IPCC Fourth Assessment Report (AR4) Climate Change 2007: The Physical Science Basis.

IPCC Fifth Assessment Report (AR5) Climate Change 2014: The Physical Science Basis.

Kiladis, G. N., M. C. Wheeler, P. T. Haertel, K. H. Straub, and P. E. Roundy, 2009: Convectively coupled equatorial waves. Rev. Geophys., 47, RG2003, doi:10.1029/2008RG000266.

Kitoh, A., 2005: Climate model simulation on the role of mountain uplift on Asian monsoon. The Geological Society of Japan, 111, XIX.

Knutson, T. R. and K. M. Weickmann, 1987: 30-60 day atmospheric oscillations: composite life cycles of convection and circulation anomalies. *Monthly Wea. Rev.* **115**, 1407-1436.

Madden, R. A. and P. R. Julian, 1994: Observations of the 40–50-day tropical oscillation—A review, *Monthly Wea. Rev.*, **122**, 814–37.

Meehl G. A., 2015: Deacadal climate variability and the early-2000s hiatus. US CLIVAR, 13, No.3, 1-6.

Saji, N. H., B. N. Goswami, P. N. Vinayachandran and T. Yamagata, 2009: A dipole mode in the tropical Indian Ocean. *Nature*, **401**, 360-363.

Trenberth, K.E and J. T. Fasllo, 2013: An apparent hiatus in global warming?. Earth's Future 1, 19-32.

Rodwell, M.J. and B. I Hoskins, 1996: Monsoons and the dynamics of deserts. *Q. J. R. Meteor. Soc.*, **122**, 1385-1404.

Webster, P. J., 1994: The role of hydrological processes in ocean-atmosphere interactions, *Review of Geophysics*, **32**,427-476.

Weng, H., K. Ashok, S. Behera, S. A. Rao and T. Yamagata, 2007: Impacts of recent El Nino Modoki on dry/wet conditions in the Pacific rim during boreal summer. *Clim Dyn.*, **29**, 113-129.

Xie, S.-P., K. Hu, J. Hafner, H. Tokinaga, Y. Du, G. Huang and T. Sampe, 2009: Indian Oceancapacitor effect on Indo-western Pacific climate during the summer following El Niño. *J. Climate*, **22**, 730-747.

Zeng, N., J. D. Neelin, K.-M. Lau and C. J. Tucker, 1999: Enhancement of interdecadal climate variability in the Sahel by vegetation interaction. *Science*, **286**, 1537-1540.

Text books

James, I. N., 1995: Introduction to Circulating Atmospheres. Cambridge University Press, 422pp.

Trenberth, K.E.(ed.), 1992: Climate System Modeling. Cambridge University Press, 788pp.

Valls G. K., 2006:Atmospheric and oceanic fluid dynamics. Cambridge University Press, 7454pp.

Wallace, J.M. and P. V. Hobbs, 2006: Atmospheric Science. Academic Press, 483pp.

Introduction of reanalysis and JRA-55

Introduction to Reanalysis and JRA-55

Masashi HARADA (Climate Prediction Division, JMA)

1. Reanalysis

Reanalysis is a scientific method to generate grid point values (GPVs) dataset for climate analysis. It is different from so-called "analysis" (Fig. 1), a process to produce initial conditions for operational numerical weather prediction (NWP) by using data assimilation (DA) system and observation data available, in two points (Fig. 2): First, the reanalysis utilizes a constant state-of-the-art NWP model and DA system for a long period, while those of the "analysis" are generally upgraded with times. Second, the reanalysis integrates all available observation including those not available at the time of operational analysis; e.g., delayed observation and reprocessed satellite data. These characteristics of the reanalysis enable us to obtain high-quality and homogeneous dataset for various meteorological variables covering the last several decades, thereby support climate services such as climate monitoring and seasonal forecasting.

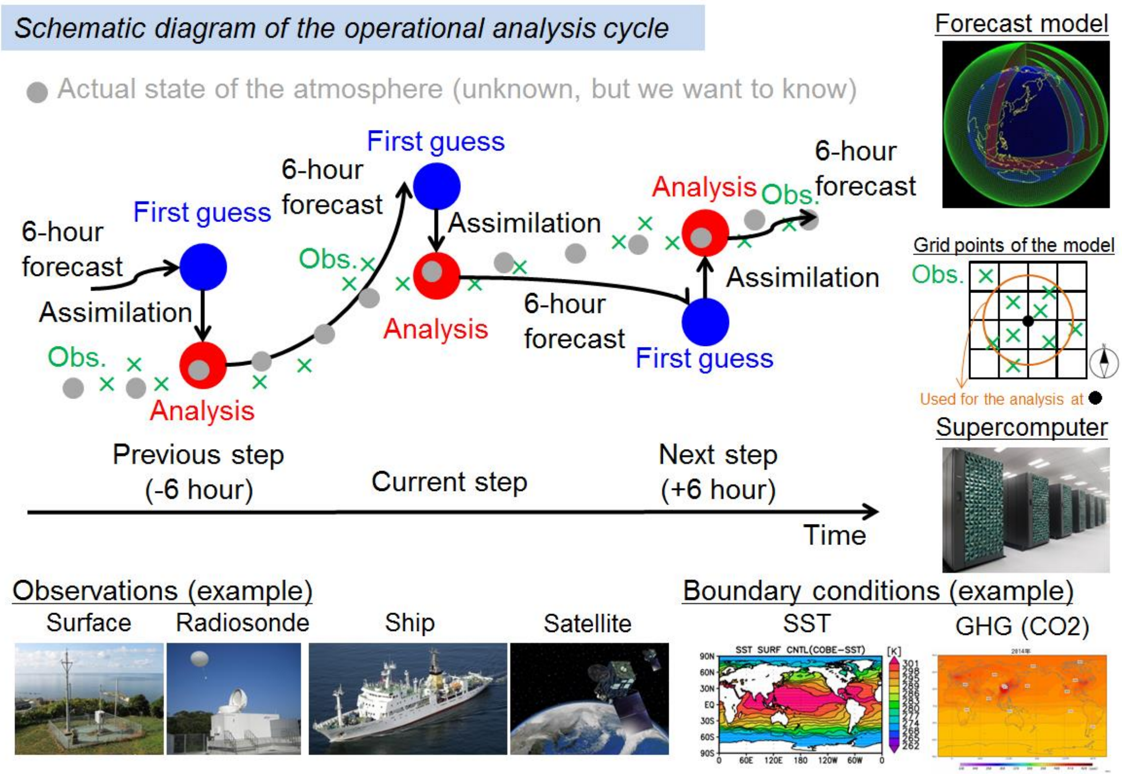

Fig. 1. Schematic diagram of operational analysis.

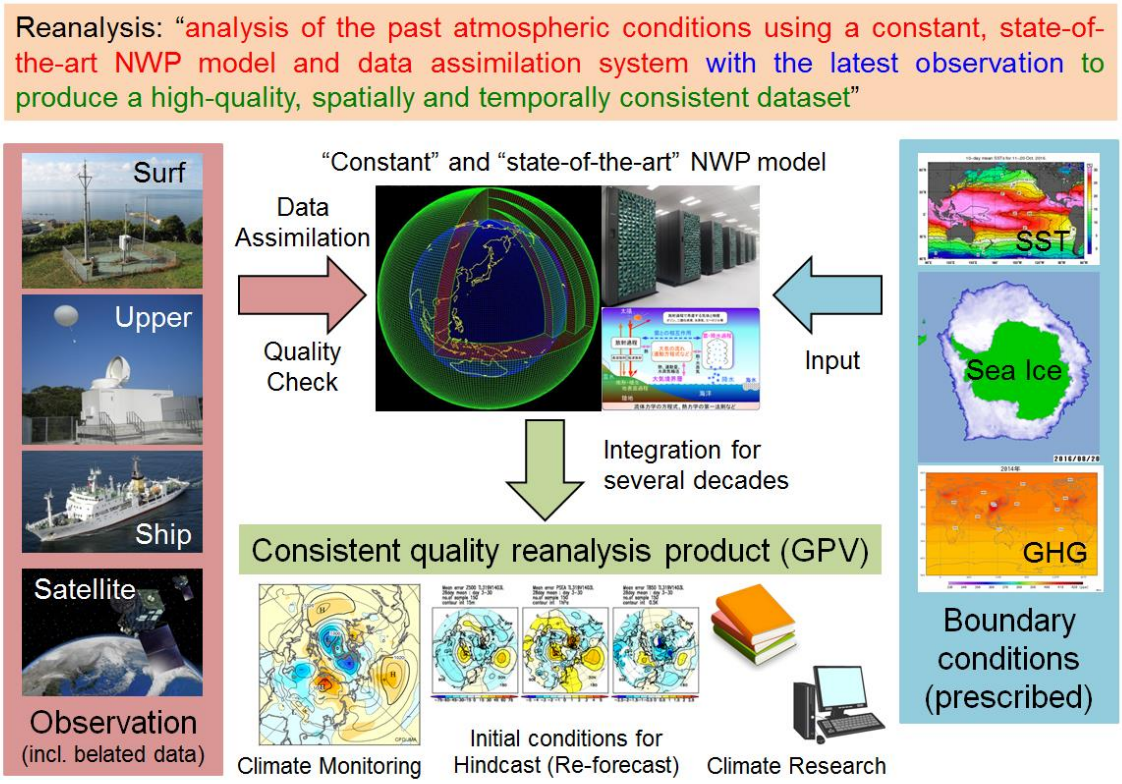

Fig. 2. Schematic diagram of reanalysis.

2. Reanalysis at JMA

Reanalysis has been conducted at a number of major NWP center. In Japan, the Japan Meteorological Agency (JMA) and the Central Research Institute of Electric Power Industry (CRIEPI) jointly produced the Japanese 25-year Reanalysis (JRA-25; Onogi et al. 2007) which covers from 1978 to 2004. In the second reanalysis by JMA called the Japanese 55-year Reanalysis (JRA-55; Kobayashi et al. 2015), updated DA system and newly prepared observations since the JRA-25 are used to improve the quality of dataset. The JRA-55 covers from 1958 to present and currently used as a basic dataset for climate services at JMA.

The JRA-55 has been produced with the TL319 version of JMA’s operational DA system as of December 2009. The NWP model is based on the TL319 spectral resolution version of the JMA Global Spectral Model (GSM) as of December 2009 (JMA 2013). Both the DA system and forecast model have been extensively improved since the JRA-25. Observations used in JRA-55 primarily consist of those used in ERA-40 (Uppala et al. 2005) and those archived by JMA. Observations after 1979 are basically the same as those used in JRA-25, but newly available observational data were collected and introduced whenever possible. Detailed list of the DA system, NWP model, and observation data are shown in tables 1, 2, and 3 of Appendix, respectively.

3. Basic performance of JRA-55

Kobayashi et al. (2015) investigated performance of JRA-55 in reproducing temporal and spatial variability of basic elements such as temperature, precipitation, and sea-level pressure. Harada et al. (2016) extended their investigation to include stratospheric circulation, tropical cyclones, the Madden-Julian oscillation, and mid-latitude storm tracks. Both studies concluded that quality of the JRA-55 improved significantly compared with that of the JRA-25. Some examples from these studies are introduced in this section.

3.1 Two-day forecast scores

Short-range forecasts using the operational analysis or reanalysis as initial conditions were conducted to evaluate the temporal consistency of each product. Figure 3 shows time series of root-mean-square errors in 2-day forecasts of a geopotential height at 500hPa averaged over the extratropical northern and southern hemisphere from the forecasts starting from JRA-25, JRA-55, and the JMA operational system, verified against their own analyses.

Two points should be pointed out: First, the scores from JRA-55 and JRA-25 are temporally steady compared with that of the operational system, indicating that quality of the operational system strongly depends on frequent upgrades of the system. Second, scores of the JRA-55 improved significantly from those of the JRA-25, which reflects updates of the system and observations since JRA-25. The improvement is particularly significant in the southern hemisphere, due to the availability of new satellite observations as well as to the improvement of the DA system.

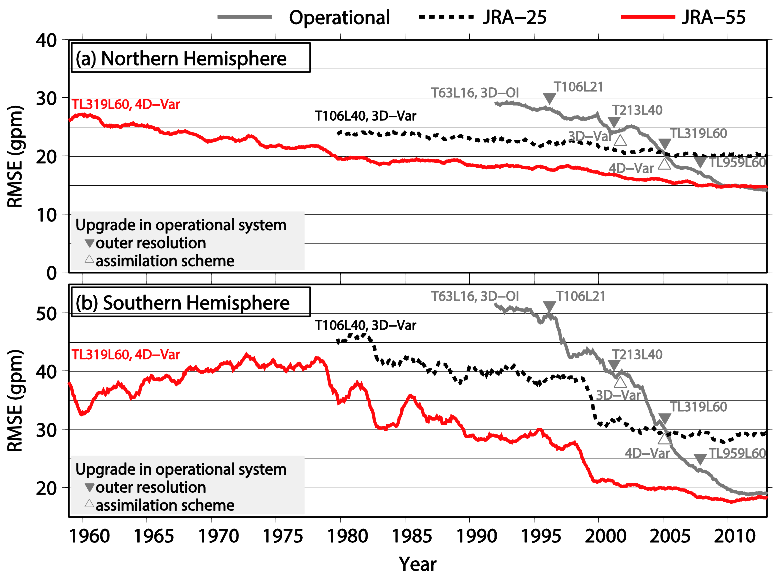

Fig. 3. RMS (Root Mean Square) errors of 2-day forecasts of the geopotential height at 500hPa averaged over the extratropics of the (a) Northern and (b) Southern Hemispheres from JRA-25, JRA-55 and JMA operational system, verified against their own analyses. Changes in the assimilation scheme and resolution of the outer model are also noted. Each value represents the average for the last 12 months.

3.2 Temperature

Figure 4 compares monthly and global mean land-surface air temperature anomalies from the Climatic Research Unit (CRU) temperature database (CRUTEM4, Jones et al. 2012), the NCEP/National Center for Atmospheric Research (NCAR) reanalysis, ERA-40, JRA-25, and JRA-55. The low-frequency variability of 2-m temperature anomalies over land is fairly comparable in two reanalysis. Compared with ERA-40, the trend reproduced in JRA-55 is closer to that in CRUTEM4 but there is a difference of less than 0.1 K between CRUTEM4 and JRA-55 after the 1990s.

The difference might be due to a difference in method to use observations between CRUTEM4 and JRA-55. In JRA-55, observations on islands and the coast are not used in the screen-level analysis of JRA-55 and analysis in those areas could be affected by observations in coastal waters such as reports of surface observation from sea stations (SHIP) and buoy observations (BUOY), and by Sea Surface Temperature (SST) through background fields. On the other hand, CRUTEM4 is based on observations over land only, which include those on islands and on the coast.

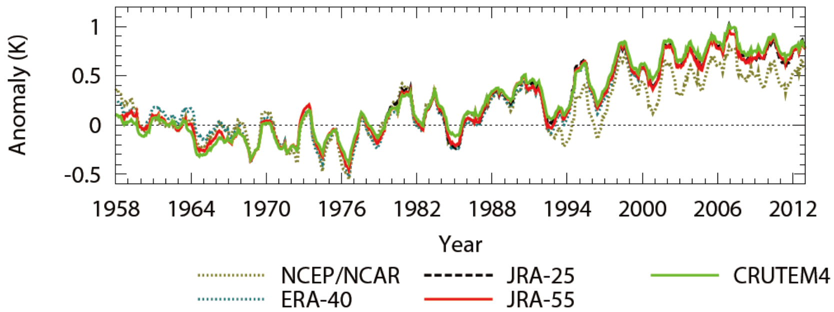

Fig. 4. Twelve-month running mean land-surface air temperature anomalies from CRUTEM4, the NCEP/NCAR reanalysis, ERA-40, JRA-25, and JRA-55, averaged over the globe. Anomalies for each dataset were defined relative to their own climatological monthly means over 1961–1990, except JRA-25, for which anomalies were first computed relative to its own climatological monthly means over 1981–2010 and then adjusted so that their average over 1979–1990 gave the same value as that of JRA-55. Reanalyses are sampled with the same spatial and temporal coverage as CRUTEM4.

3.3 Precipitation

Figure 5 shows the climatological distribution of precipitation in JRA-55, JRA-25, ERA-Interim (Dee et al. 2011), ERA-40, the Modern-Era Retrospective Analysis for Research and Applications (MERRA, Rienecker et al. 2011), and the Global Precipitation Climatology Project (GPCP) version 2.2 (Adler et al. 2003) as an observational dataset. While precipitation in middle and high latitudes are underestimated in most reanalysis, JRA-55 well reproduce these feature, especially in the Pacific and Atlantic Oceans north of 30°N. On the other hand, JRA-55 overestimates precipitation in the tropics compared with GPCP. The regions where JRA-55 overestimates precipitation tend to exhibit the spin-down problem[1] (not shown). Therefore, the excessive precipitation in the tropics in JRA-55 is most likely related to the dry bias and the spin-down problem of the forecast model in regions of deep convection.

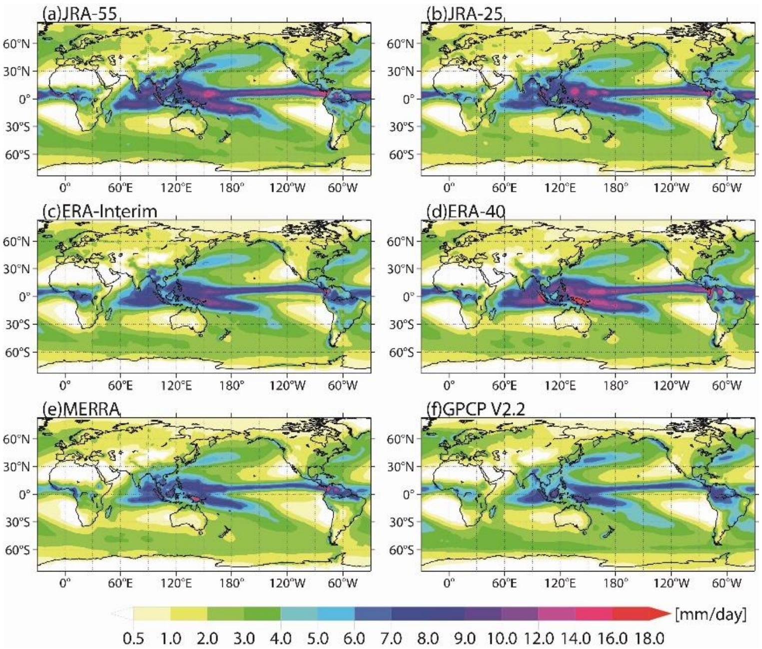

Fig. 5. Climatological annual mean precipitations in (a) JRA-55, (b) JRA-25, (c) ERA-Interim, (d) ERA-40, (e) MERRA, and (f) GPCP V2.2, averaged over 1980–2001.

4. JRA-55 user application and homepage

The JRA-55 data are available from the JMA Data Distribution System (JDDS) for registered users. Registration application can be made at the JRA-55 homepage by filling in necessary information such as name, affiliation, and purpose of use. The dataset is also available from the Data Integration and Analysis System (DIAS) managed by the University of Tokyo, the Center for Computational Sciences (CCS) of University of Tsukuba, NCAR in the U.S.A., and the Earth System Grid Federation (ESGF) at the National Aeronautics and Space Administration (NASA). Note that registration at the JRA-55 homepage is valid only at JDDS and separate registration is required for downloading from these collaborative organizations.

The JRA-55 homepage also provides detailed information on data (JRA-55 Product User's Handbook) and its quality issues. In addition, the homepage displays climate maps for a variety of meteorological variables ranging from basic metrics to technical considerations for climate research (JRA-55 Atlas). It is expected to be widely useful in research and education.

JRA-55 homepage: http://jra.kishou.go.jp/JRA-55/index_en.html
JRA-55 Atlas: http://ds.data.jma.go.jp/gmd/jra/atlas/en/index.html

[1] Precipitation is excessive immediately after the start of forecasts and then gradually decreases.

5. Next Japanese reanalysis: JRA-3Q

JMA is currently planning the third Japanese reanalysis called JRA-3Q (Japanese Reanalysis for Three Quarters of a century), which covers over 75 years from around 1947 to present. The JRA-3Q will be produced by utilizing the latest NWP and DA system as of 2018, as well as newly added observation since the JRA-55, to update quality of the reanalysis products. The calculation will be started in the first quarter of 2019 and ended by the end of 2021. Detail of the provisional plan and schedule will be presented in the lecture.

Appendix: Detail of the DA system, NWP model, and observation data for JRA-25 and JRA-55.

Table 1. Data assimilation systems used for JRA-25 and JRA-55.

	JRA-25	**JRA-55**
Basic system	JMA's operational system as of March 2004 (JMA 2002)	JMA's operational system as of December 2009 (JMA 2007, 2013b)
Horizontal grid system	Gaussian	Reduced Gaussian
Horizontal resolution	T106 (~110 km)	TL319 (~55 km)
Atmospheric analysis		
Vertical levels	Surface and 40 levels up to 0.4 hPa	Surface and 60 levels up to 0.1 hPa (Iwamura and Kitagawa 2008; Nakagawa 2009)
Analysis scheme	3D-Var with the T106 inner resolution	4D-Var with the T106 inner resolution
Background error covariances	Static	Static with the simple inflation factor of 1.8 applied before 1972
Bias correction for satellite radiances	*TOVS* Adaptive scheme using 1D-Var analysis departures (Sakamoto and Christy 2009) *ATOVS* Static (until July 2009) and adaptive (thereafter) schemes using radiosonde and supplemental background fields (Kazumori et al. 2004)	VarBC (Derber and Wu 1998; Dee and Uppala 2009; JMA 2013)
Radiative transfer model for satellite radiances	*TOVS:* RTTOV-6 *ATOVS:* RTTOV-7	RTTOV-9.3
Surface analysis		
Screen-level analysis	2D-OI	2D-OI with the FGAT approach
Land surface analysis	Offline SiB with 6-hourly atmospheric forcing	Offline SiB with 3-hourly atmospheric forcing
Snow depth analysis	2D-OI	2D-OI

Table 2. Forecast models used for JRA-25 and JRA-55.

	JRA-25	**JRA-55**
Base model	JMA GSM as of March 2004 (JMA 2002)	JMA GSM as of December 2009 (JMA 2007, 2013b)
Horizontal resolution	T106 (~110 km)	TL319 (~55 km)
Vertical levels	Surface and 40 levels up to 0.4 hPa	Surface and 60 levels up to 0.1 hPa (Iwamura and Kitagawa 2008; Nakagawa 2009)
Dynamics		
Horizontal grid system	Gaussian	Reduced Gaussian

Advection scheme	Euralian	Semi-Lagrangian
Radiation		
Longwave radiation	*Line absorptions* Random band model of Goody (1952) *Water vapor continuum (e-type)* Roberts et al. (1976) *Radiatively active gases* H_2O, O_3 and CO_2 (constant at 375 ppmv)	*Line absorptions* Pre-computed transmittance tables and *k*-distribution (Chou et al. 2001) *Water vapor continuum (e-type and p-type)* Zhong and Haigh (1995) with MK_CKD (Clough et al. 2005) *Radiatively active gases* H_2O, O_3, CO_2, CH_4, N_2O, CFC-11, CFC-12 and HCFC-22
Shortwave radiation	*Absorptions by H_2O, O_2, O_3 and CO_2* Briegleb (1992)	*Absorptions by H_2O* Briegleb (1992) *Absorptions by O_2, O_3 and CO_2* Freidenreich and Ramaswamy (1999)
Cloud radiation	*Longwave* Maximum-random overlap *Shortwave* Random overlap	*Longwave* Maximum-random overlap with the method of Räisänen (1998) *Shortwave* Random overlap
Aerosols	Atmospheric aerosol profiles from WMO (1986) (CONT-I over land and MAR-I over sea)	Atmospheric aerosol profiles from WMO (1986) (CONT-I over land and MAR-I over sea) with optical depths adjusted to 2-dimensional monthly climatology
Cumulus convection	Prognostic Arakawa-Schubert	Prognostic Arakawa-Schubert with DCAPE
Initialization	Nonlinear normal mode initialization	Not used
Boundary conditions and forcing fields		
SST and sea ice	COBE-SST (Ishii et al. 2005)	COBE-SST (Ishii et al. 2005)
Ozone	T42L45 version of MRI-CCM1 (Shibata et al. 2005)	*Until 1978:* Climatology *From 1979 onward:* T42L68 version of MRI-CCM1 (Shibata et al. 2005)

Table 3. Observational data sources for JRA-55. Observations shown in plain cells were added or reprocessed after JRA-25, whereas those in shaded cells are the same as those used in JRA-25. Acronyms in this table are summarized in Appendix B. of Kobayashi et al. (2015).

Data supplier	Data type and supplier's identifiers	Period	Note
Conventional data			
ECMWF		Jan 1958-Aug 2002	Uppala et al. (2005)
JMA		Jan 1961-	
	GAME and SCSMEX	Apr 1998-Oct 1998	
NCEP/NCAR	SYNOP and upper-level observation	Jan 1979-Dec 1979	Kalnay et al. (1996) Kistler et al. (2001)
M. Yamanaka	Radiosondes from Indonesia	Jan 1958-	Okamoto et al. (2003)
M. Fiorino	TCRs	Jan 1958-	Fiorino (2002)
RIHMI	Snow depths from Russia	Jan 1958-Dec 2008	
UCAR	Snow depths from USA	Jan 1958-Aug 2011	NCDC et al. (1981)
Monthly Surface Meteorological Data in China	Snow depths from China	Jan 1971-Dec 2006	Digitized from printed matters
IMH	Snow depths from Mongolia	Jan 1975-Dec 2007	
Satellite radiances			
ECMWF	VTPR	Jan 1973-Feb 1976	Uppala et al. (2005)
	HIRS and SSU	Nov 1978-Dec 2000	
	MSU and AMSU	Nov 1978-May 2003	
NOAA/NCDC	SSM/I	Jun 1987-Dec 2004	
NOAA/CLASS	AMSU and MHS	Aug 1998-	
	SSM/I	Jul 1987-	

JMA	AMSU and MHS	Jun 2003-	
	SSM/I and SSMIS	Mar 2006-	
	TMI	Dec 2011-	
	CSR	Jun 2005-	
JMA/MSC	Reprocessed CSRs from GMS-5, GOES 9 and MTSAT-1R	Jul 1995-Dec 2009	
JAXA, NASA	Reprocessed TMI version 7	Feb 1998-Dec 2011	
JAXA	Reprocessed AMSR-E Version 3	Jun 2002-Oct 2011	
EUMETSAT	CSRs from the Meteosat series	Jan 2001-Aug 2009	
AMVs			
ECMWF	GMS, Meteosat and GOES	Jan 1979-Dec 1997	Uppala et al. (2005)
JMA	GMS, MTSAT, Meteosat and GOES	Dec 1979-Dec1980, Jan 1998-	
	MODIS	Jun 2004-	
JMA/MSC	Reprocessed GMS, GOES 9 and MTSAT-1R	Jan 1979-Nov 1979 Nar 1987-Sep 2009	
EUMETSAT	Reprocessed Meteosat-2	May 1982-Aug 1988	van de Berg et al. (2002)
	Reprocessed Meteosat-3 and -7	Jan 1989-Dec 2000 Aug 1988-Nov 1998	
	Meteosat-5 and -7	Jan 2001-Feb 2001	
Scatterometer ocean surface winds			
ESA	Reprocessed AMI (ERS.ASPS20.N)	May 1997-Jan2001	De Chiara et al. (2007)
Hersbach (2008)			
JPL	Reprocessed SeaWinds from QuickSCAT (QSCAT_LEVEL_2B_V2)	Jul 1999-Nov 2009	Dunbar et al. (2006)
JMA	ASCAT	Jan 2008-	
GNSS-RO refractivities			
CDAAC	Reprocessed CHAMP, SAC-C, COSMIC, GRACE, Metop-A, TerraSAR-X, and C/NOFS	Jul 2006-Jun 2012	
JMA	COSMIC, GRACE, Metop, TerraSAR-X, and C/NOFS		

References

Adler, R.F., G. J. Huffman, A. Chang, R. Ferraro, P.-P. Xie, J. Janowiak, B. Rudolf, U. Schneider, S. Curtis, D. Bolvin, A. Gruber, J. Susskind, P. Arkin, and E. Nelkin, 2003: The Version-2 Global Precipitation Climatology Project (GPCP) monthly precipitation analysis (1979-present). J. Hydrometeor., 4, 1147-1167.

Briegleb, B. P., 1992: Delta-Eddington approximation for solar radiation in the NCAR community climate model. J. Geophys. Res., 97, 7603–7612.

Chou, M.-D., M. J. Suarez, X.-Z. Liang, and M. M.-H. Yan, 2001: A thermal infrared radiation parameterization for atmospheric studies. Technical report series on global modeling and data assimilation, NASA/TM-2001-104606, 19, National Aeronautics and Space Administration (NASA) Goddard Space Flight Center, USA, 68 pp.

Clough, S. A., M. W. Shephard, E. J. Mlawer, J. S. Delamere, M. J. Iacono, K. Cady-Pereira, S. Boukabara, and P. D. Brown, 2005: Atmospheric radiative transfer modeling: a summary of the AER codes. J. Quant. Spectrosc. Radiat. Transfer, 91, 233–244.

De Chiara, G., R. Crapolicchio, and P. Lecomte, 2007: ERS-1/2 scatterometer new products: mission reprocessing and data quality improvement. Paper presented at the 2nd Space for Hydrology Workshop, Geneva, Switzerland, November, 12-14, 2007.

Dee, D. P., S. M. Uppala, A. J. Simmons, P. Berrisford, P. Poli, S. Kobayashi, U. Andrae, M. A. Balmaseda, G. Balsamo, P. Bauer, P. Bechtold, A. C. M. Beljaars, L. van de Berg, J. Bidlot, N. Bormann, C. Delsol, R. Dragani, M. Fuentes, A. J. Geer, L. Haimberger, S. B. Healy, H. Hersbach, E. V. Hólm, L. Isaksen, P. Kållberg, M. Köhler, M. Matricardi, A. P. McNally, B. M. Monge-Sanz, J.-J. Morcrette, B.-K. Park, C. Peubey, P. de Rosnay, C. Tavolato, J.-N. Thépaut, and F. Vitart, 2011: The ERA-Interim reanalysis: configuration and performance of the data assimilation system. Quart. J. Roy. Meteor. Soc., 137, 553-597.

Dunbar, R. S., T. Lungu, B. Weiss, B. Stiles, J. Huddleston, P. S. Callahan, G. Shirtliffe, K. L. Perry, C. Hsu, C. Mears, F. Wentz, and D. Smith, 2006: QuikSCAT science data product user's manual. Version 3.0, D-18053 - Rev A, Jet Propulsion Laboratory (JPL), USA, 85 pp.

Fiorino, M., 2002: Analysis and forecasts of tropical cyclones in the ECMWF 40-year reanalysis (ERA-40). 25th Conference on Hurricanes and Tropical Meteorology, CA, USA, 261–264.

Freidenreich, S. M., and V. Ramaswamy, 1999: A new multiple-band solar radiative parameterization for general circulation models. J. Geophys. Res., 104, 31389–31409.

Goody, R. M., 1952: A statistical model for water-vapour absorption. Quart. J. Roy. Meteor. Soc., 78, 165–169.

Harada, Y., H. Kamahori, C. Kobayashi, H. Endo, S. Kobayashi, Y. Ota, H. Onoda, K. Onogi, K. Miyaoka, and K. Takahashi, 2016: The JRA-55 Reanalysis: Representation of atmospheric circulation and climate variability, J. Meteor. Soc. Japan, 94, 269-302.

Iwamura, K., and H. Kitagawa, 2008: An upgrade of the JMA operational global NWP model. CAS/JSC WGNE Res. Activ. Atmos. Oceanic Modell., 38, 3–4.

Ishii, M., A. Shouji, S. Sugimoto, and T. Matsumoto, 2005: Objective analyses of sea-surface temperature and marine meteorological variables for the 20th century using ICOADS and the KOBE collection. Int. J. Climatol., 25, 865–879.

JMA, 2002: Outline of the operational numerical weather prediction at the Japan Meteorological Agency. WMO Numerical Weather Prediction Progress Report. JMA, Japan, 158 pp.

JMA, 2007: Outline of the operational numerical weather prediction at the Japan Meteorological Agency. WMO Technical Progress Report on the Global Data-Processing and Forecasting System and Numerical Weather Prediction, JMA, Japan, 194 pp.

JMA, 2013: Outline of the operational numerical weather prediction at the Japan Meteorological Agency. Appendix to WMO Technical Progress Report on the Global Data-processing and Forecasting System (GDPFS) and Numerical Weather Prediction (NWP) Research, JMA, Japan, 188 pp.

Jones, P. D., D. H. Lister, T. J. Osborn, C. Harpham, M. Salmon, and C. P. Morice, 2012: Hemispheric and large-scale land surface air temperature variations: An extensive revision and an update to 2010. J. Geophys. Res., 117, D05127, doi:10.1029/2011JD017139.

Kalnay, E., M. Kanamitsu, R. Kistler, W. Collins, D. Deaven, L. Gandin, M. Iredell, S. Saha, G. White, J. Woollen, Y. Zhu, M. Chelliah, W. Ebisuzaki, W. Higgins, J. Janowiak, K. C. Mo, C. Ropelewski, J. Wang, A. Leetmaa, R. Reynolds, R. Jenne, and D. Joseph, 1996: The NCEP/NCAR 40-year reanalysis project. Bull. Amer. Meteor. Soc., 77, 437–471.

Kazumori, M., H. Owada, and K. Okamoto, 2004: Improvements of ATOVS radiance-bias correction scheme at JMA. CAS/JSC WGNE Res. Activ. Atmos. Oceanic Modell., 34, 15–16.

Kistler, R., E. Kalnay, W. Collins, S. Saha, G. White, J. Woollen, M. Chelliah, W. Ebisuzaki, M. Kanamitsu, V. Kousky, H. van den Dool, R. Jenne, and M. Fiorino, 2001: The NCEP-NCAR 50-year reanalysis: Monthly means CD-ROM and documentation. Bull. Amer. Meteor. Soc., 82, 247–267.

Kobayashi, S., Y. Ota, Y. Harada, A. Ebita, M. Moriya, H. Onoda, K. Onogi, H. Kamahori, C. Kobayashi, H. Endo, K. Miyaoka, and K. Takahashi, 2015: The JRA-55 reanalysis: General specifications and basic characteristics. J. Meteor. Soc. Japan, 93, 5–48.

Nakagawa, M., 2009: Outline of the high resolution global model at the Japan Meteorological Agency. RSMC Tokyo-Typhoon Center Technical Review, 11, JMA, Japan, 1–13.

NCDC, NWS, and FAA, 1981: NCDC TD3200 U.S. cooperative summary of day, 1890(1948)-cont. Research Data Archive at NCAR, Computational and Information Systems Laboratory, USA.

Okamoto, N., M. D. Yamanaka, S.-Y. Ogino, H. Hashiguchi, N. Nishi, T. Sribimawati, and A. Numaguchi, 2003: Seasonal variations of tropospheric wind over Indonesia: comparison between collected operational radiosonde data and NCEP reanalysis for 1992–99. J. Meteor. Soc. Japan, 81, 829–850.

Onogi, K., J. Tsutsui, H. Koide, M. Sakamoto, S. Kobayashi, H. Hatsushika, T. Matsumoto, N. Yamazaki, H. Kamahori, K. Takahashi, S. Kadokura, K. Wada, K. Kato, R. Oyama, T. Ose, N. Mannoji, and R. Taira, 2007: The JRA-25 reanalysis. J. Meteor. Soc. Japan, 85, 369-432.

Rienecker M. M., M. J. Suarez, R. Gelaro, R. Todling, J. Bacmeister, E. Liu, M. G. Bosilovich, S. D.

Schubert, L. Takacs, G.-K. Kim, S. Bloom, J. Chen, D. Collins, A. Conaty, A. da Silva, W. Gu, J. Joiner, R. D. Koster, R. Lucchesi, A. Molod, T. Owens, S. Pawson, P. Pegion, C. R. Redder, R. Reichle, F. R. Robertson, A. G. Ruddick, M. Sienkiewicz, and J. Woollen. 2011: MERRA: NASA’s Modern-Era Retrospective Analysis for Research and Applications. J. Climate, 24, 3624-3648.

Räisänen, P., 1998: Effective longwave cloud fraction and maximum-random overlap of clouds: a problem and a solution. Mon. Wea. Rev., 126, 3336–3340.

Roberts, R. E., J. E. A. Selby, and L. M. Biberman, 1976: Infrared continuum absorption by atmospheric water vapor in the 8-12-μm window. Appl. Opt., 15, 2085–2090.

Shibata, K., M. Deushi, T. T. Sekiyama, and H. Yoshimura, 2005: Development of an MRI chemical transport model for the study of stratospheric chemistry. Pap. Geophys. Meteor., 55, 75–119.

Uppala, S. M., P. W. Kållberg, A. J. Simmons, U. Andrae, V. Da Costa Bechtold, M. Fiorino, J. K. Gibson, J. Haseler, A. Hernandez, G. A. Kelly, X. Li, K. Onogi, S. Saarinen, N. Sokka, R. P. Allan, E. Andersson, K. Arpe, M. A. Balmaseda, A. C. M. Beljaars, L. Van De Berg, J. Bidlot, N. Bormann, S. Caires, F. Chevallier, A. Dethof, M. Dragosavac, M. Fisher, M. Fuentes, S. Hagemann, E. Hólm, B. J. Hoskins, L. Isaksen, P. A. E. M. Janssen, R. Jenne, A. P. McNally, J.-F. Mahfouf, J.-J. Morcrette, N. A. Rayner, R. W. Saunders, P. Simon, A. Sterl, K. E. Trenberth, A. Untch, D. Vasiljevic, P. Viterbo, and J. Woollen, 2005: The ERA-40 re-analysis. Quart. J. Roy. Meteor. Soc., 131, 2961-3012.

van de Berg, L., J. Gustafsson, and A. Yildirim, 2002: Reprocessing of atmospheric motion vectors from Meteosat image data. ECMWF ERA-40 Project Report Series, 3, ECMWF, UK, 159–168.

WMO, 1986: A preliminary cloudless standard atmosphere for radiation computation, World Climate Programme (WCP), 112, 53 pp.

Zhong, W., and J. D. Haigh, 1995: Improved broadband emissivity parameterization for water vapor cooling rate calculations. J. Atmos. Sci., 52, 124–138.

Seasonal Forecast

Seasonal Forecast

Hiroshi Ohno
Tokyo Climate Center (TCC)/
Climate Prediction Division of
Japan Meteorological Agency (JMA)

Outline

- Introduction
- Predictability and Ensemble Prediction
- Seasonal Forecast in Japan
- Procedure of Seasonal Forecast

Introduction

Short/Long Range Forecasts

Short range forecast

(/: to, |: occasionally or partly)

Tokyo Chiho	Three-hourly Forecasts	Probability of Precipitation	Temperature Forecast
Today 21 November	CLEAR	00-06 --% 06-12 0% 12-18 0% 18-24 0%	Tokyo Daytime High 12°C
Tomorrow 22 November	CLOUDY, OCCASIONAL SCATTERED SHOWERS LATER	00-06 0% 06-12 10% 12-18 20% 18-24 50%	Tokyo Morning Low 3°C, Daytime High 13°C

- Forecasting the actual weather parameters (e.g., weater, temp.)
- Deterministic forecast

Seasonal forecast

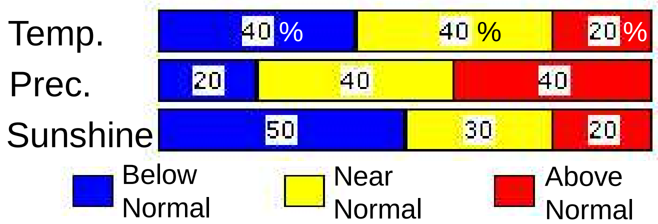

Above example shows a forecast in 3 categories: **Below**, **Near** and **Above normal**.

Probabilities of both below and near normal temp. are **40%**, and above normal temp. is **20%**.

- Forecasting deviation from the climatological normal in categories (Not actual temp. or precip.)
- Probabilistic forecast (Not forecasting which category will happen, but forecasting probabilities of occurrence for each category)

Anomaly in Seasonal Forecast

Normal: Defined as 30-year average for 1981 – 2010
Anomaly: Deviation from the normal
[Anomaly] = [Actual Value] – [Normal]

- Weather condition changes from year to year (interannual variability)
- Anomalous climate may affects the lives of society (e.g., drought, flood, and hot spell)

Anomaly is the target of seasonal forecasting.

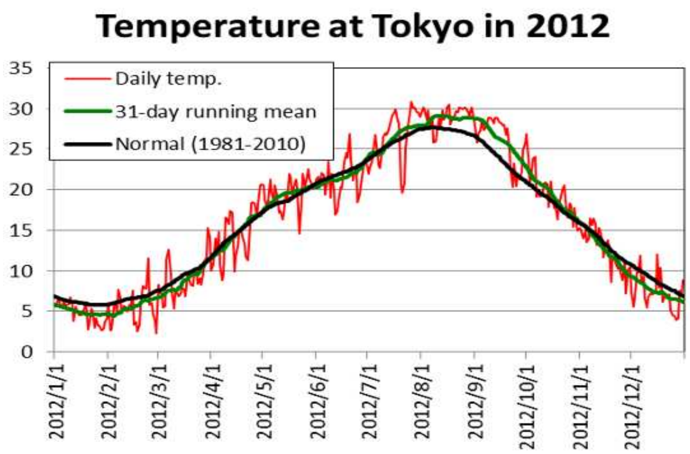

Forecast Category

- JMA conducts seasonal forecast in **3 categories**: **Above**, **Near**, and **Below Normal**
- Arranging historical data for 30-year (e.g., 1981-2010) in ascending order,
  - 1 - 10th: **Below Normal**
  - 11 - 20th: **Near Normal**
  - 21 - 30th: **Above normal**

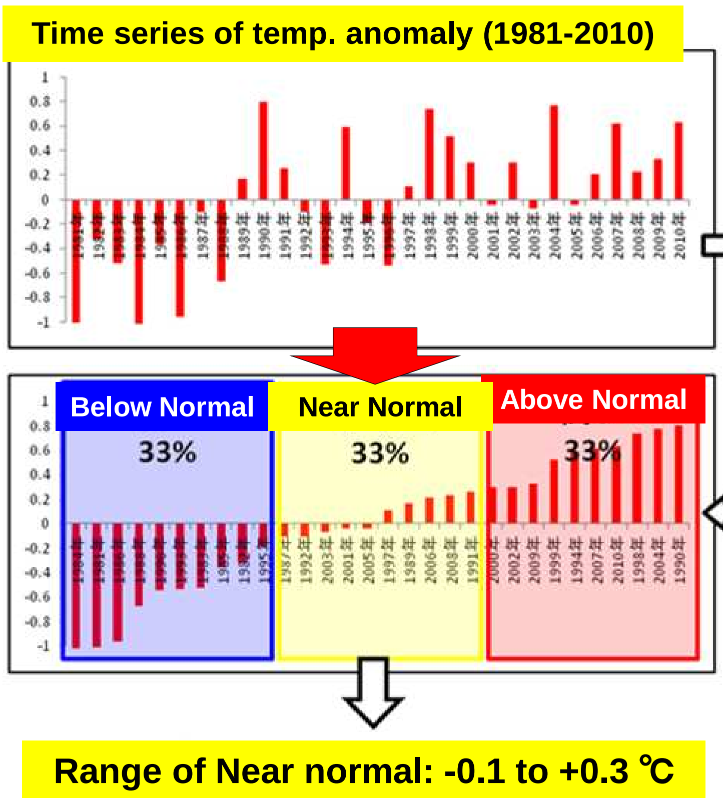

3-category Probabilistic Forecast

- In the seasonal forecast probability for each category is predicted.
- Occurrence rate for each category is expected 33% in climatology.
- In certain forecasting, deviation from the climatological occurrence is important.

Climatological occurrence

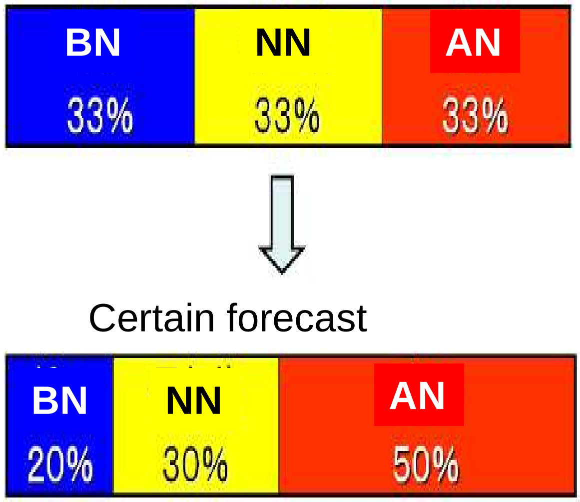

This forecast shows that above normal is ***more likely*** (50%), and below normal is ***less likely*** (20%) to occur than expected in climatology (33%).

Predictability and Ensemble Prediction

Multiple Structure of Atmospheric Phenomena

- Variations in atmosphere consist various space- and time-scale phenomena.
- Targets for seasonal prediction are phenomena with large time- and space-scale (over about a month).

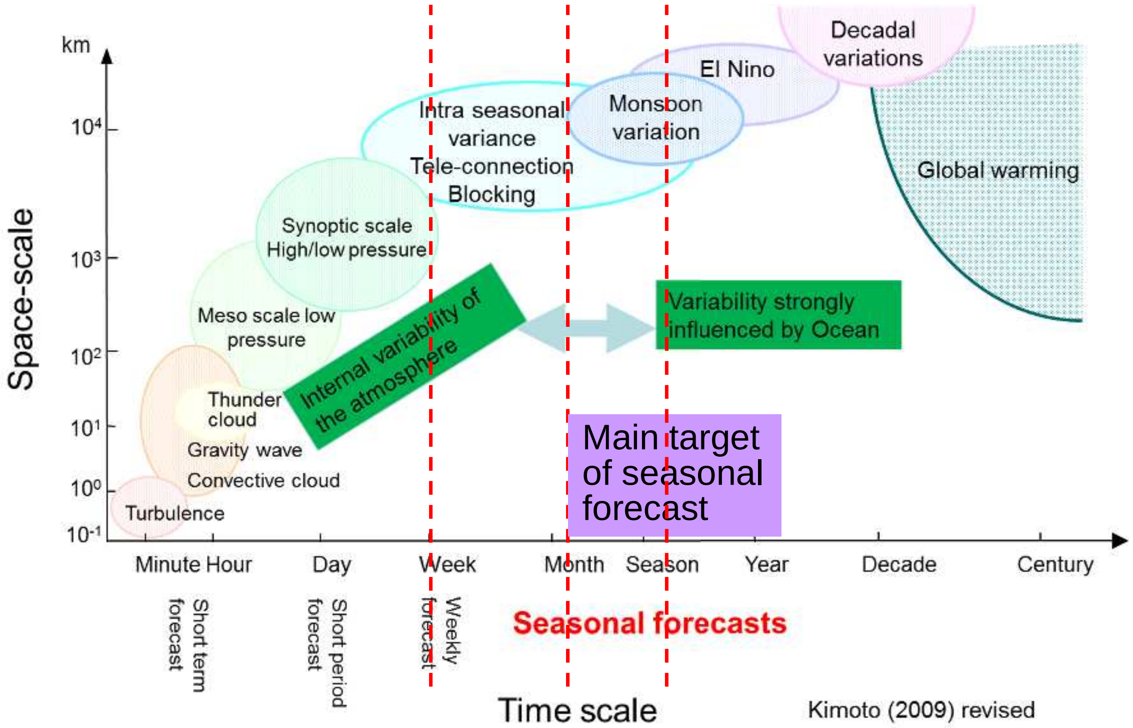

Signal and Noise for Each Kind of Forecast

Green boxes show signal for short-range forecast and noise for one-month forecast

Kind of forecast	**Signal**	**Noise**
Medium-range (One-week forecast)	Shortwave disturbance dominating over daily variations of weather	
Extended –range (One-month forecast)	Low-frequency variation of atmosphere (meanderings of the jet, blocking, AO, MJO and so on)	Transient eddies (moving high, low)
Long-range (Three-month, Warm/Cold season forecast)	Low-frequency variation of tropical ocean and its influence, such as ENSO and Indian Ocean variation	Low-frequency variation of atmosphere

Blue box shows signal for seasonal forecast

Red boxes show signal for one-month forecast and noise for seasonal forecast

Noise can be reduced by time average (e.g., 3-month mean)

Chaos in Atmosphere

- Due to chaotic behavior of atmosphere, errors rapidly grow during period of prediction.

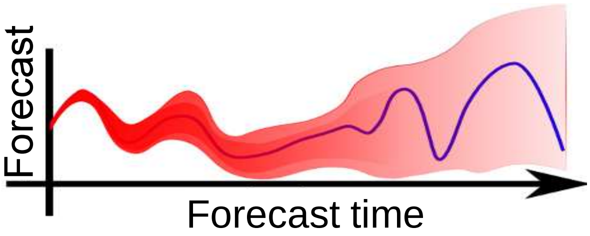

- To address this issue, ensemble prediction is essential for long-range forecasting.

Ensemble Prediction

In **ensemble prediction**, the model is run many times from very slightly different initial conditions.

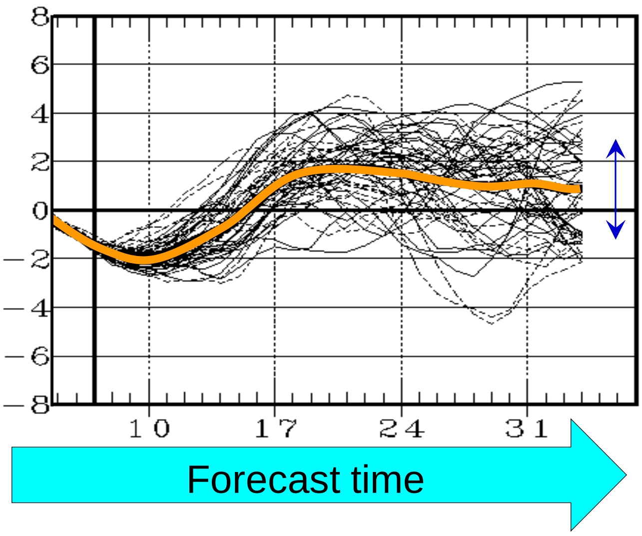

Ensemble Member = Individual solutions

Ensemble spread = Standard dev. among members, suggesting degree of **uncertainty**

Ensemble mean = Average of ensemble members, suggesting degree of **signal**

- Ensemble mean is statistically better than each member.
- The more the number of members is, the better the prediction is.

Deterministic and Probabilistic Forecast

Deterministic forecast

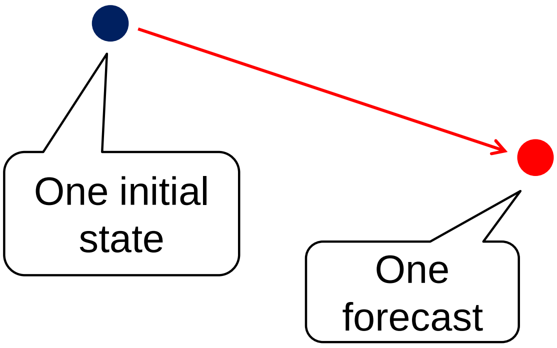

Calculate one forecast using one initial state

Probabilistic forecast

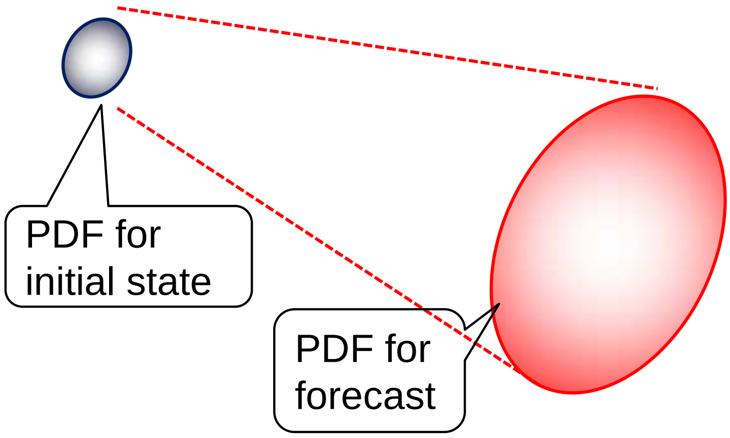

- EPS derives PDF for forecast.
  - ➢Possible to predict probability of the targeted phenomena, which add degree of reliability to deterministic forecasting.

Probabilistic Forecast

- Ensemble prediction system (EPS) enables to derive PDF from the distribution of individual members.
- This denotes that long-range forecast is possible with not deterministic but probabilistic manner.

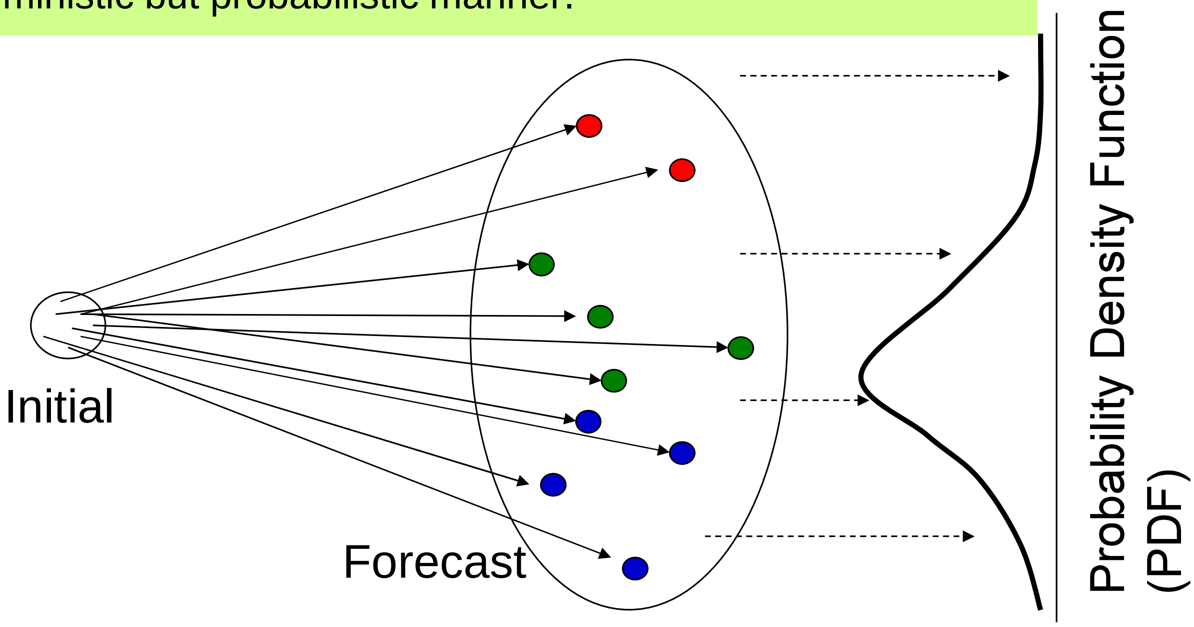

Initial and Boundary Condition

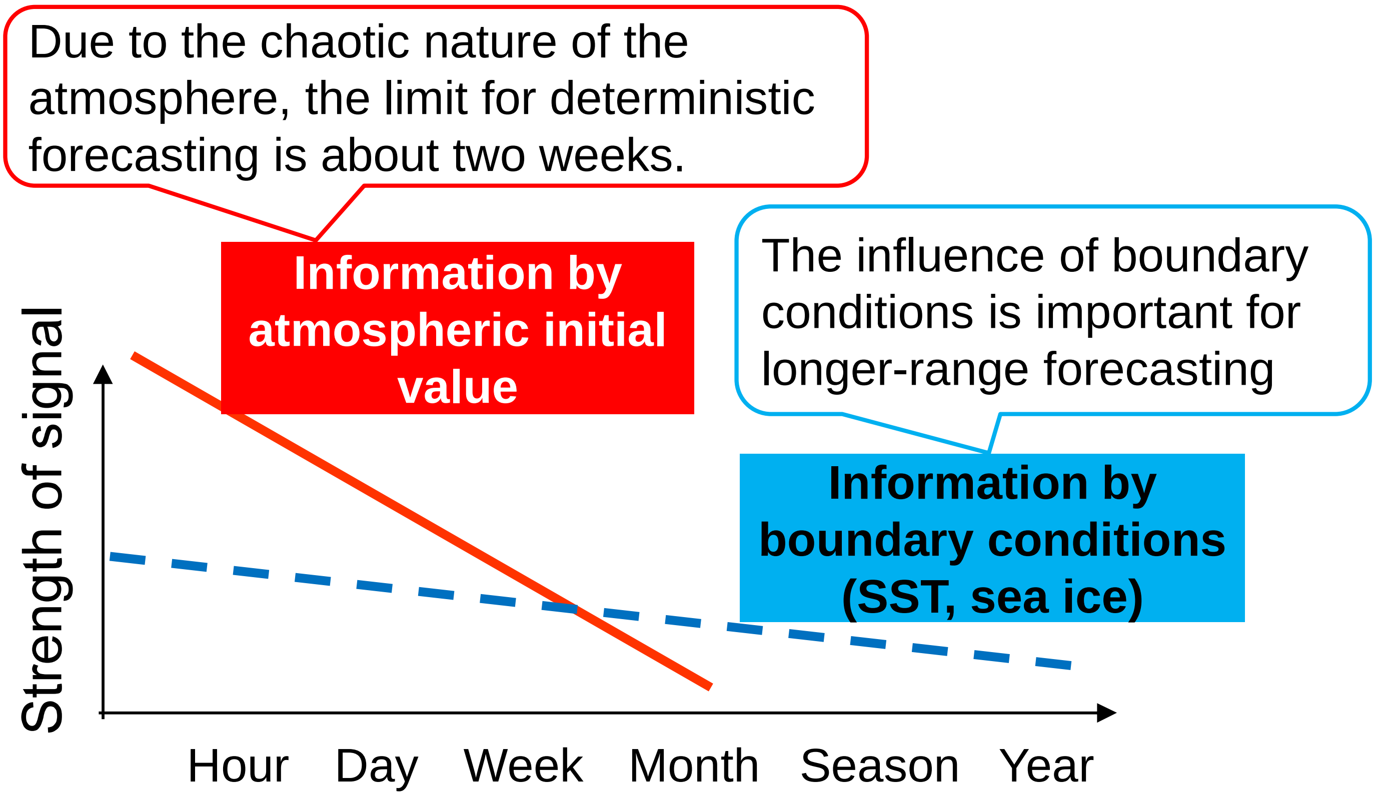

Boundary Condition – ENSO

- ENSO brings large impact on the global climate.
- Its evolution is predictable several month ahead.
- Its timescale is several month to a year.

➡ ENSO is the most important BC for seasonal forecast.

Typical anomaly patterns during **El Nino** (boreal winter)

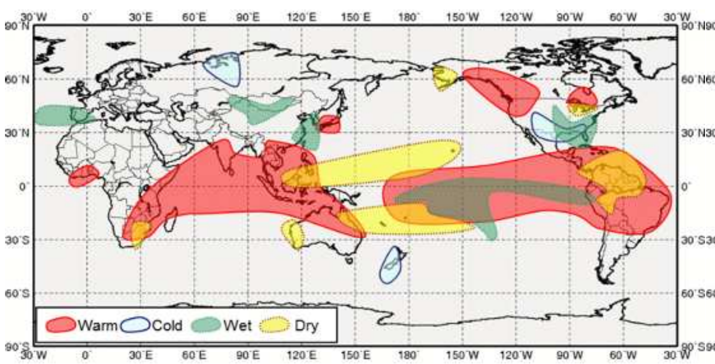

Typical anomaly patterns during **La Nina** (boreal winter)

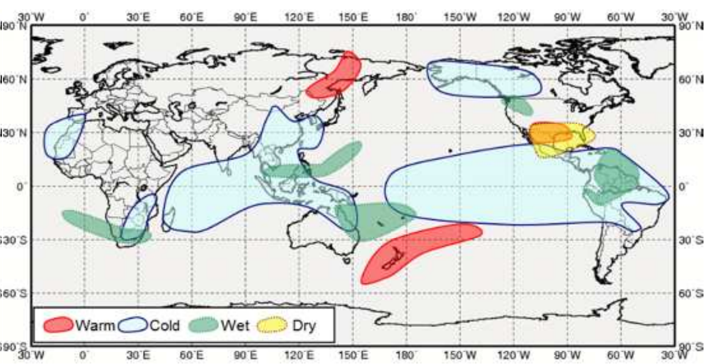

Boundary Condition – ENSO

- Typical anomaly pattern (**signal**) tends to appear during El Nino (or La Nina), but not always due to the internal variability (**noise**).
- Seasonal forecast must be issued with probabilistic forecast because of the uncertainty from the noise.

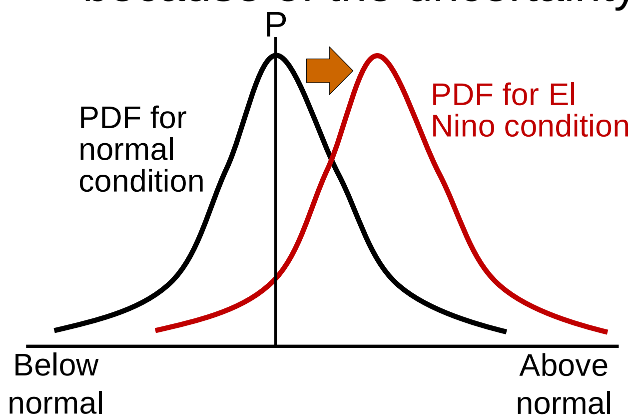

In this case, El Nino brings more (less) probability for above (below) normal category than normal condition

Ratio (signal / (signal + noise)

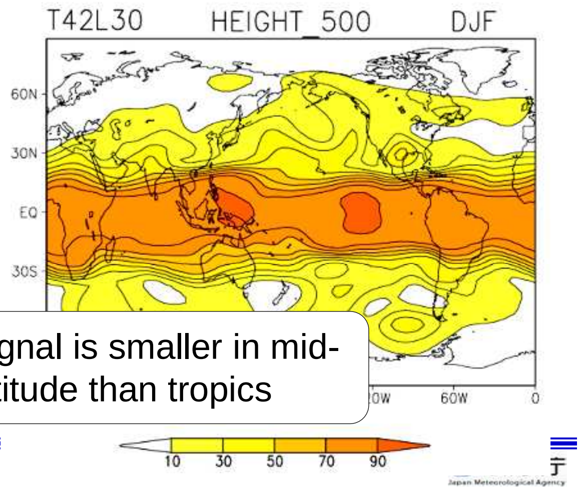

Signal is smaller in mid-latitude than tropics

Seasonal Forecasts in Japan

Japan's seasonal forecast started in 1942 for the purpose to reduce agricultural damages associated with cooler summers.

Seasonal Forecast at JMA

	Date of issue	Forecast Period	Forecast Item
1-month Forecast	Every Thursday	1-month mean	Temperature, Precipitation, Sunshine, Snowfall
		Weekly mean (1st, 2nd, 3rd-4th week)	Temperature
3-month Forecast	Around 25th of every month	3-month mean,	Temperature, Precipitation, Snowfall
		Monthly mean (1st, 2nd, 3rd month)	Temperature, Precipitation
Warm Season Forecast	Around 25 Feb.	3-month mean (Jun. – Aug.)	Temperature, Precipitation
		Rainy season (Jun. – Jul.)	Precipitation
Cold Season Forecast	Around 25 Sep.	3-month mean (Dec. – Feb.)	Temperature, Precipitation, Snowfall

Forecast Region

- Forecast is issued for sub-regions divided based on the climate characteristics.

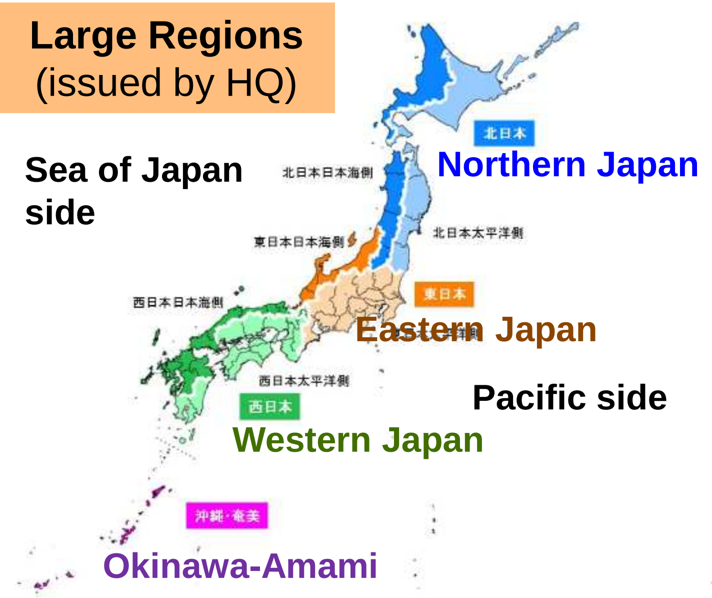

One-month Forecast

Example issued on 30 Nov. 2017

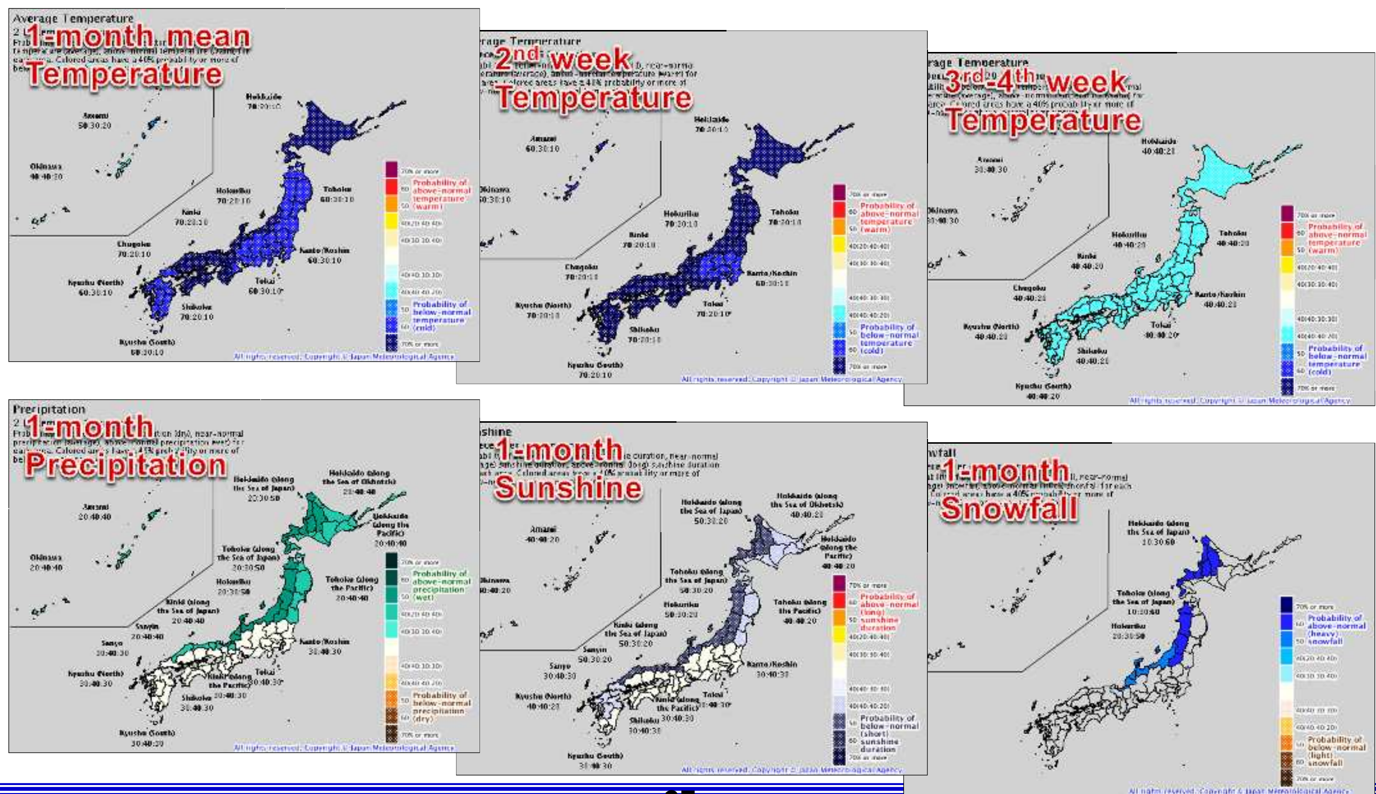

Three-month Forecast

Example issued on 24 Nov. 2017

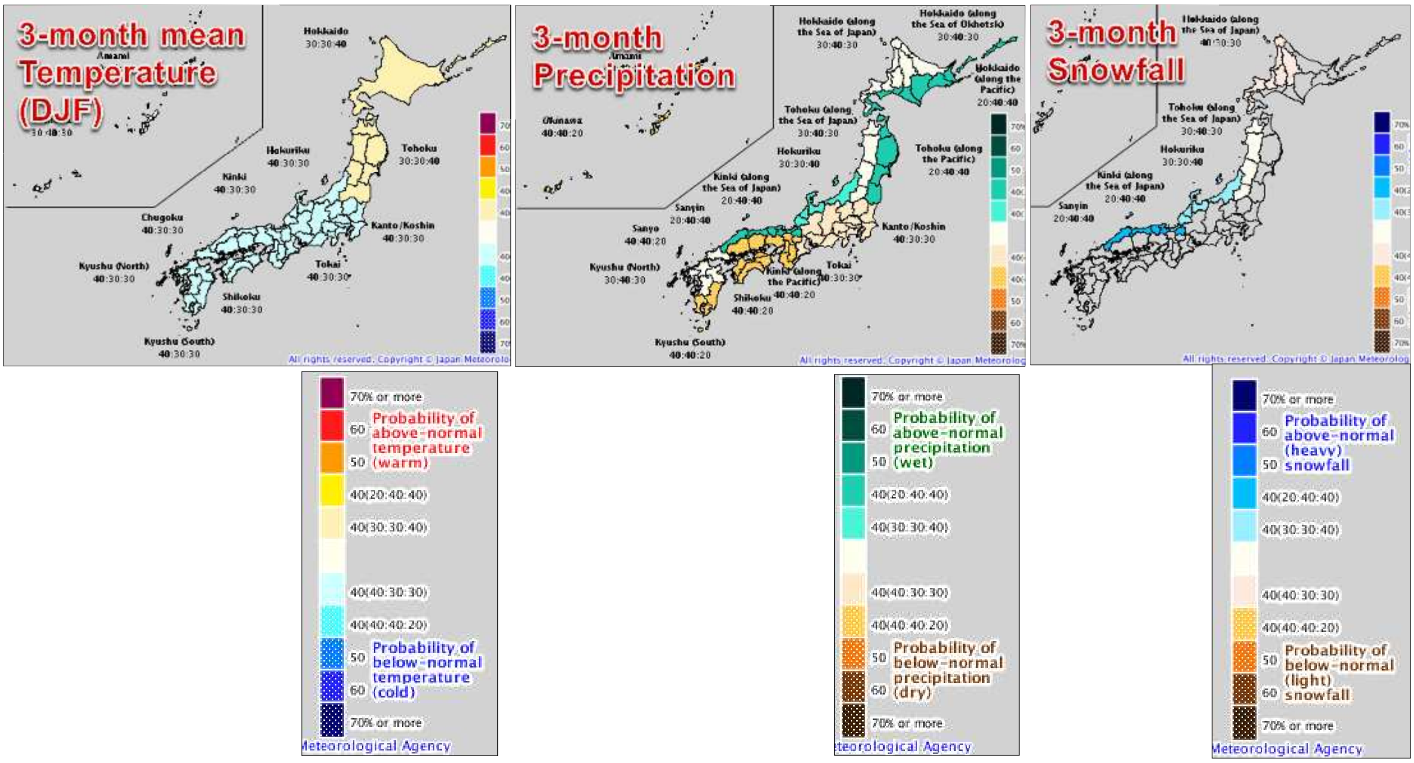

Commentary on 3-month Forecast

Commentary material is also provided from JMA HP

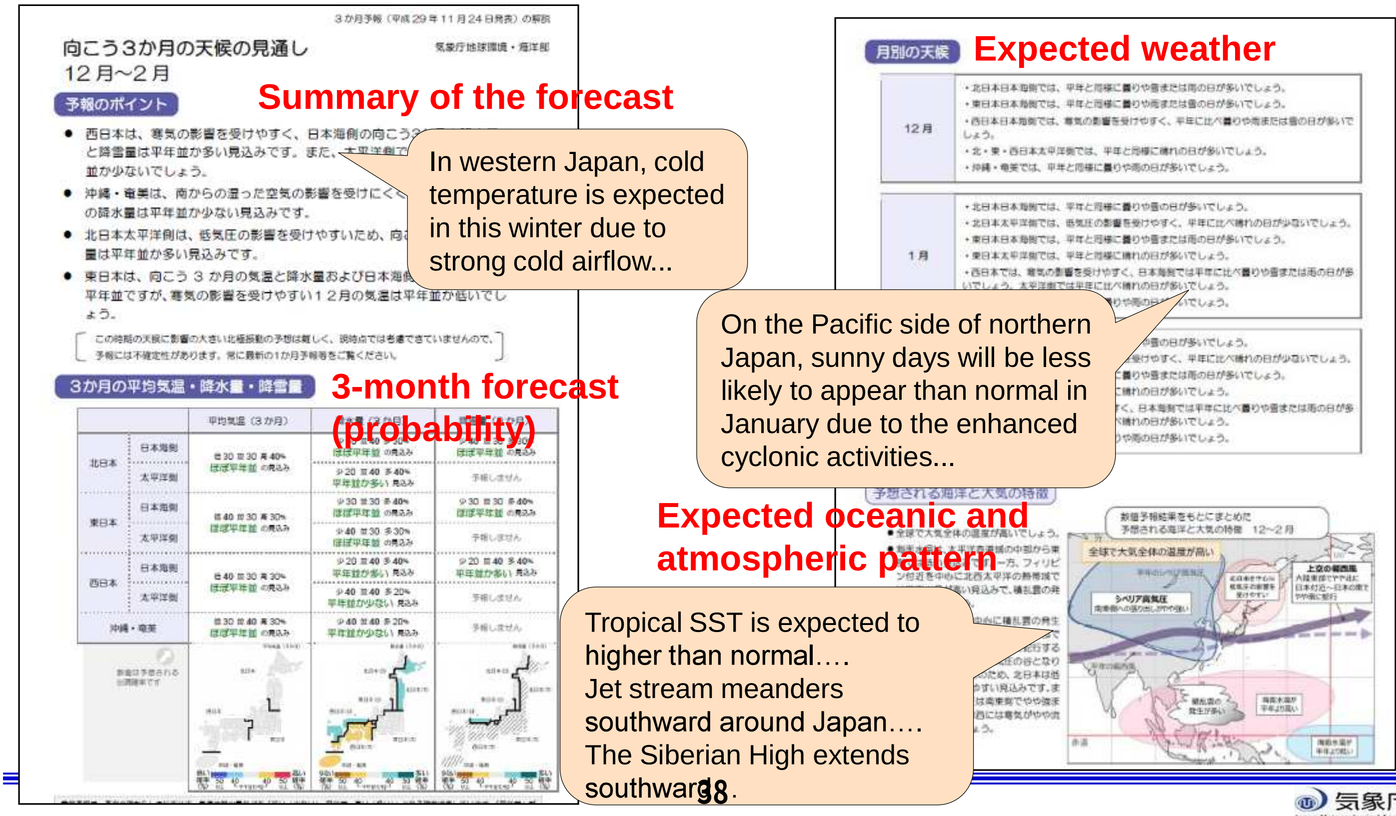

Early Warning Information for Extreme Weather

- **Objective**: Mitigation of the adverse impacts from extreme weather events (hot/cold spell, heavy snow) on socio-economic activities such as agriculture and disaster prevention in early stage (1-2-week ahead).
- **Targeted event**: An extreme 7-day averaged temperature or 7-day snowfall amounts event which appears once per decade in climatology (i.e., 10%).
- **Timing of issuing**: When targeted event is expected to happen 5-14-day ahead with the probability of 30% or more (i.e., 3 times more likely to happen than normal).

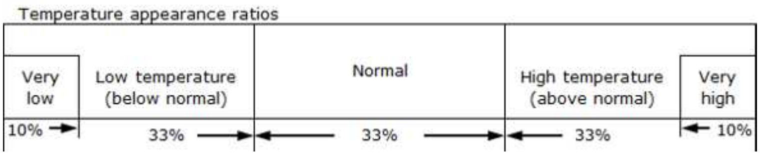

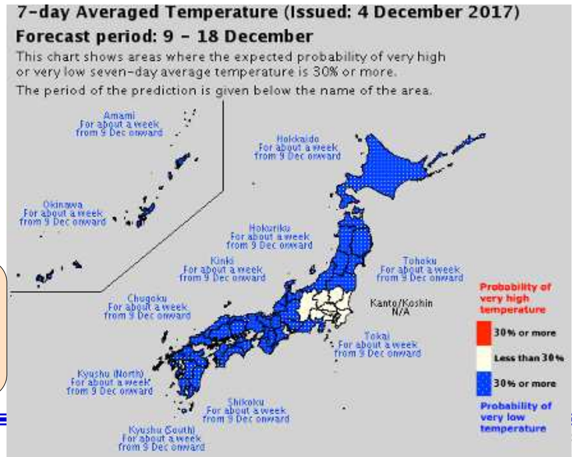

In this example, information for significantly cold weather from 9 Dec. onward was issued on 4 Dec.

Utilization of Seasonal Forecast

JMA is promoting the utilization of long-range forecast (mainly 2-week/1-month prediction) in various sectors such as agriculture.

Examples

- Prediction data is used at local governments to estimate the adequate timing of rice and fruit harvesting.
- Advisory information is provided by a research organization to reduce damage from significant cold/hot weather on rice farming.

Procedure of Seasonal Forecast

Flow of Making Seasonal Forecast

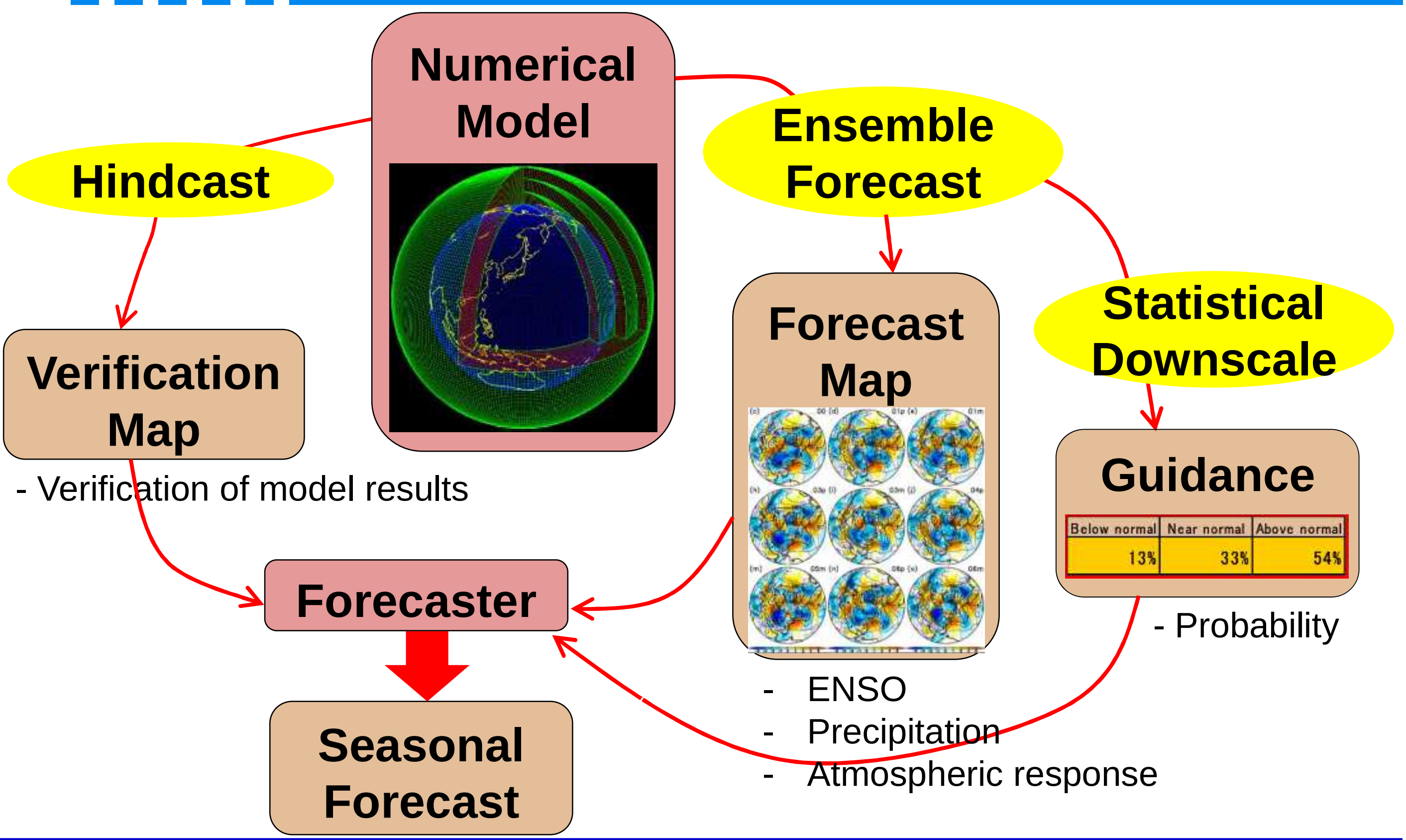

Procedure of Seasonal Forecast (1)

1. Understand the current status of ocean and atmosphere
2. Check the numerical model results

   Exercise on Thursday

   – SST in the tropics (ENSO, Indian Ocean,…)
   – Convective activity (Precipitation)
   – Atmospheric circulation (response to the convection)
3. Check the prediction skill of the numerical model
   – Which model results should be taken to the forecast?

These will be introduced during the seminar…

Products for seasonal forecast provided at TCC-HP

- **Forecast Map**
- **Monthly Discussion**
- **Hindcast Verification Charts**
- **El Nino Outlook**

Procedure of Seasonal Forecast (2)

4. Check the **guidance** to estimate probability
5. Decide forecast

   Goal of this seminar

   – Modify the guidance based on the prediction skill of the model results and the guidance

Exercise on Wednesday

Guidance is an application to translate model output values into target of forecasting with statistical relationship between forecast and observation

INPUT

Numerical model

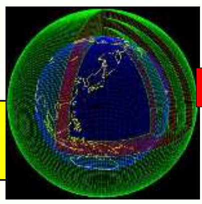

Statistical downscale

OUTPUT

Probabilistic forecast

Variability in the tropical oceans

Variability in the tropical oceans

Jun'ichi HIROSAWA
Climate Prediction Division, Japan Meteorological Agency (JMA)

1. Introduction

Tropical oceans play major roles in global climate variability. Atmosphere-ocean coupled phenomena in the tropical oceans induce global atmospheric and oceanic circulations that affect regional climate variability. On the interannual time scale, El Niño/Southern Oscillation (ENSO) of the tropical Pacific is known as a typical example of such phenomena. Recently, terms of "El Niño Modoki" or "Central Pacific (CP) El Niño" are used to distinguish them from canonical El Niño events or Eastern Pacific (EP) El Niño. Variability of the tropical Indian Ocean such as Indian Ocean Basin Wide (IOBW) and Indian Ocean Dipole (IOD) modes also impacts on global climate, especially the Asian and African climate.

2. El Niño/Southern Oscillation (ENSO)

Interannual variability in the Pacific is dominated by El Niño/Southern Oscillation (ENSO), which has its largest signature in the tropics. This phenomenon appears primarily to be the result of interactions between the tropical oceans and overlying atmosphere (Philander 1990), and thus produces sea surface temperature (SST) and heat content anomalies that are concentrated in the tropics.

El Niño (La Niña) event is a phenomenon that an area of warmer (cooler)-than-normal SST persists in the central and eastern parts of the equatorial Pacific for 6 to 18 months. Figure 1 shows SST distributions in December in normal years and El Niño years (2012 and 2015, respectively). In December 2015, waters warmer than normal are seen from around the date line

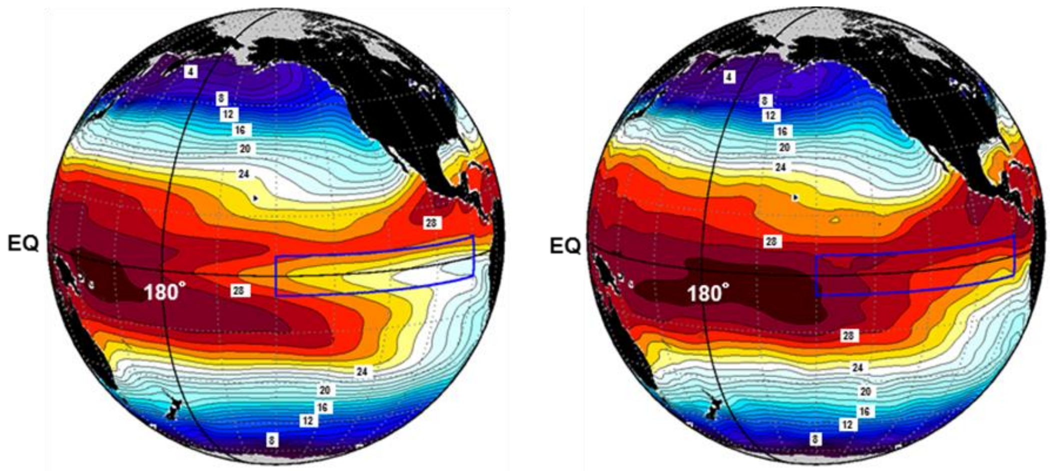

Figure 1 Monthly mean sea surface temperature in December in 2012 (normal year: left) and 2015 (El Niño year: right). Rectangle area indicates the El Niño monitoring region (NIÑO.3: 5°S-5°N, 150°-90°W).

This content is based on Yasuda 2016.

to the west coast of Peru in the equatorial Pacific. During an El Niño event, the region of SST above 28˚C, which is related to active evaporate for the sea, extends eastward, and the precipitation area shifts eastward 6,000-12,000 km.

Figure 2 shows schematic diagrams of zonal sections of atmospheric and oceanic conditions along the equatorial Pacific during a normal period, an El Niño event and a La Niña event. During an El Niño event (bottom left panel), the trade wind is weaker than normal and surface warm water spreads further east than normal. SST pattern in December 2015 shown in the right of Figure 1 reveals this feature. The active convection area shifts eastward associated with this change in SST pattern. During a La Niña event (bottom right panel of Figure 2), atmospheric and oceanic conditions seen in the normal years are reinforced. Trade wind is stronger, atmospheric convection is more active in the western Pacific. More warm waters are accumulated in the western Pacific and more cold waters move upward in the eastern Pacific due to the stronger trade wind. In other words, El Niño and La Niña events are the large scale atmospheric-ocean coupled phenomena that changes in the zonal gradient of ocean temperature and Walker circulation due to zonal shift of active convection area are impact each other.

In the developing stage of ENSO, a positive feedback of atmosphere-ocean coupled interaction, i.e., Bjerknes feedback is an essential mechanism (Bjerknes, 1999). For mechanisms of the quasi-periodic oscillation of ENSO, two major theories, i.e., the delayed oscillator (Schopf and Suarez, 1988; Suarez and Schopf, 1988) and the recharge-discharge oscillator (Jin, 1997a, b) have been proposed. The delayed oscillator explains El Niño developing due to the

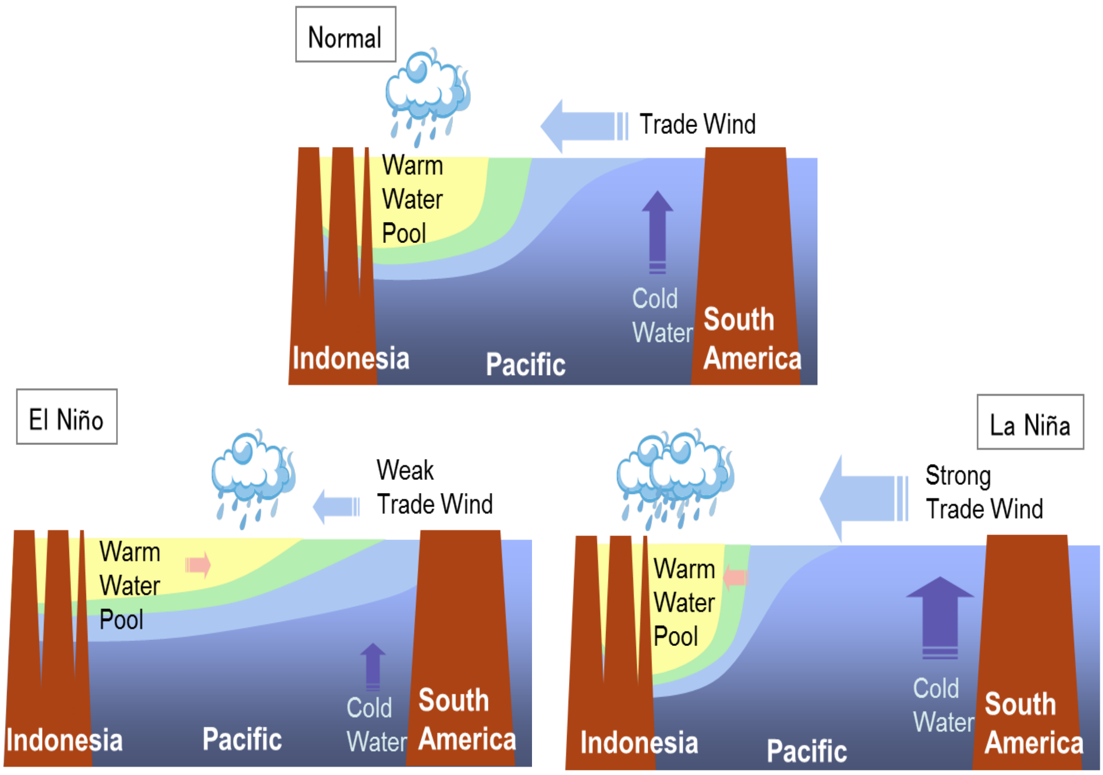

Figure 2 Schematic views of atmospheric and oceanic conditions in the equatorial Pacific during a normal condition (top), an El Niño event (bottom left), and a La Niña event (bottom right).

downwelling Kelvin wave and Bjerknes feedback, and El Niño terminating due to upwelling Kelvin wave resulting from the westward propagating Rossby wave reflected at the western boundary (Figure 3). Recharge-discharge oscillator emphasizes the major role of the storage of equatorial heat and how that leads to a self-sustaining oscillation shown in Figure 4.

ENSO affect the global atmospheric circulation, and cause extreme weather events all over the world. Figure 5 shows schematic charts of typical anomaly patterns of surface temperature and precipitation for boreal summer and winter in past El Niño/La Niña events.

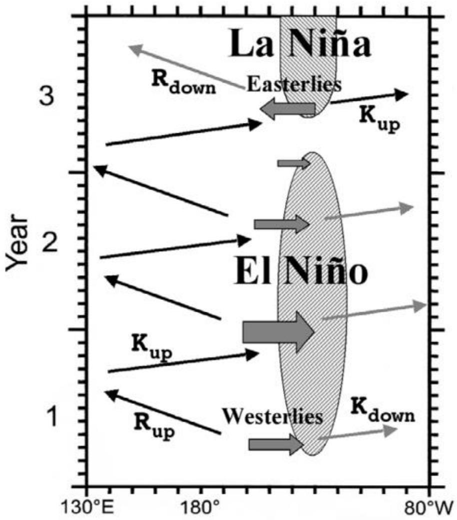

Figure 3 Schematic time-longitude diagram of the delayed oscillator theory for ENSO. From Wang and Picaut (2004).

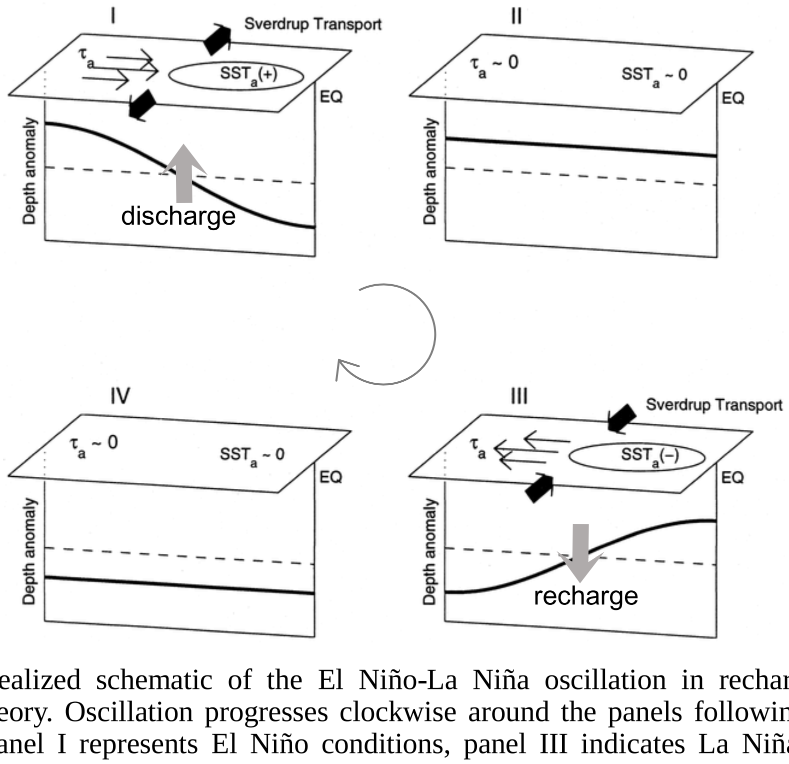

Figure 4 Idealized schematic of the El Niño-La Niña oscillation in recharge-discharge oscillator theory. Oscillation progresses clockwise around the panels following the roman numerals; panel I represents El Niño conditions, panel III indicates La Niña conditions. From Meinen and McPhaden (2000).

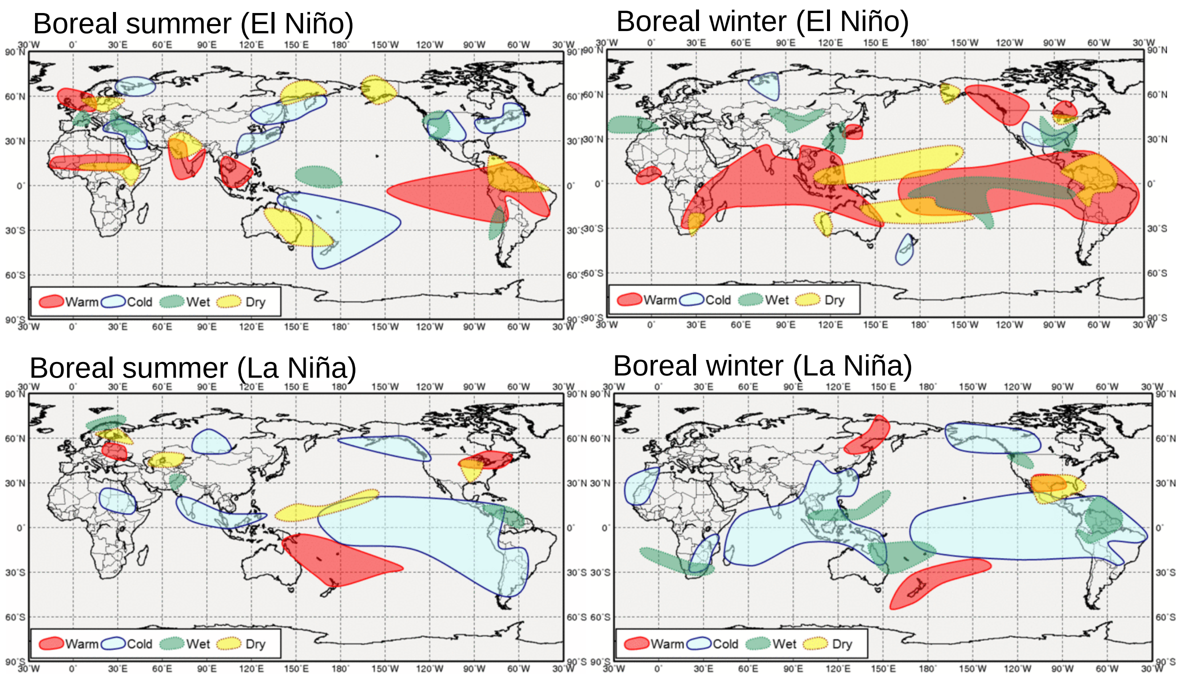

Figure 5 Schematic charts of typical anomaly patterns of surface temperature and precipitation for boreal summer and winter in past El Niño/La Niña events based on the observation and Japanese 55-year Reanalysis (JRA-55) data from 1958 through 2012.

3. 2014-16 El Niño event

The Japan Meteorological Agency (JMA) monitors SST in the NIÑO.3 region (5°S–5°N, 150°W–90°W), where interannual variability is the largest in the equatorial Pacific, to identify El Niño/La Niña events. In JMA, El Niño (La Niña) events are defined such that the five-month running mean of NIÑO.3 SST deviation from the latest 30-year average continues +0.5 (-0.5) °C or higher (lower) for six consecutive months or longer. According to this definition, the 2014-16 El Niño event started to develop in boreal summer 2014 (Figure 6). However, five-month running mean of NIÑO.3 SST deviation remained slightly above +0.5 °C of El Niño thresholds until boreal winter 2014/2015 (December 2014 - February 2015). This event strengthened from boreal spring 2015, and the NIÑO.3 SST deviation recorded its peak value of +3.0 °C in December 2015 (Figures 6 and 7). Thereafter, it decayed rapidly and terminated in boreal spring 2016. Duration seasons of this event were 8 seasons (boreal summer 2014 - boreal spring 2016), which is the longest among 15 El Niño events that have occurred since 1949.

The 2014-16 El Niño event was the strongest for 18 years since the El Niño event in 1997-98. During this event, monthly mean NIÑO.3 SST recorded +3.0°C above the latest 30-year average in December 2015. Among fifteen El Niño events that have occurred since 1949, the value of +3.0˚C was third to the two strongest previous El Niño events in 1997-98 and 1982-83 (+3.6 and +3.3 °C, respectively; Figure 8).

The annual anomaly of the global average surface temperature in 2016 was +0.45°C above the 1981-2010 average, and was the highest since 1891. Global average surface temperature is affected by natural climate variability on interannual to interdecadal time scales in addition to the global warming due to increasing of greenhouse gasses such as CO_2. Since the global

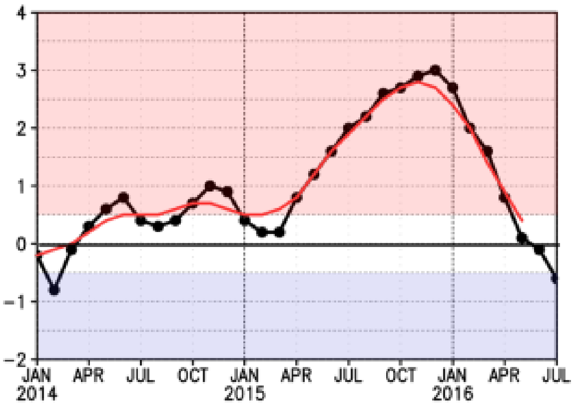

Figure 6 Time series of NIÑO.3 SST deviation from the latest 30-year average (°C). Black (red) line indicates monthly mean (five-month running mean).

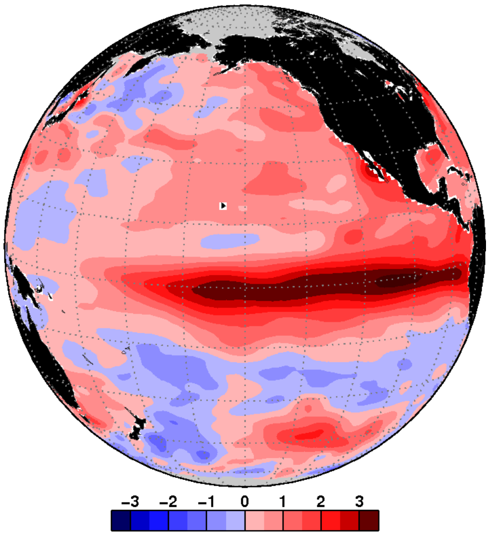

Figure 7 Monthly mean SST in December 2015 (peak of the El Niño event) relative to 1981-2010 mean. Units are °C.

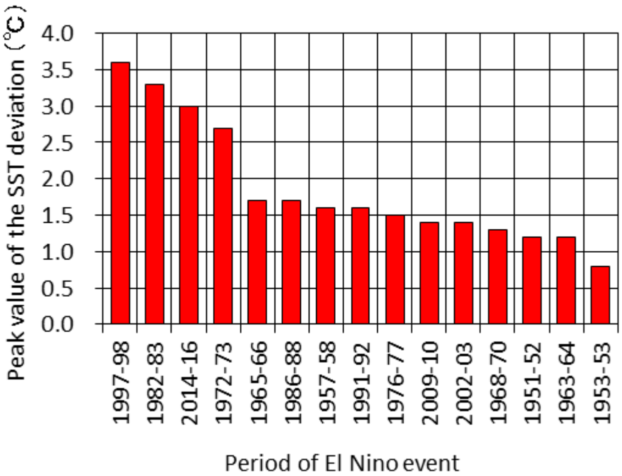

Figure 8 Peak values of NIÑO.3 SST deviation during each El Niño event since 1949 (°C). The deviation is a departure from the latest 30-year average in each event.

average surface temperature anomaly varies with a time lag of several months to NIÑO.3 SST anomaly, the highest temperature record in 2016 could be influenced by the El Niño that began in boreal summer 2014 and continued until boreal spring 2016.

The 2014-16 El Niño event also can be considered to affected to climate in Asia-Pacific region from boreal summer 2015 to boreal winter 2015/2016, high temperatures in low latitudes as well as low precipitations in and around Indonesia. India and Pakistan were suffered from heat waves in May and June 2015, respectively. Six-months-mean temperature from July to December 2015 for Hyderabad in southern India was 27.4°C that was 2.2°C higher than the normal. The total precipitation amount from September to November 2015 in Banjarmasin in Borneo Island of Indonesia was 113mm that was 19% to the normal. These events were consistent with typical anomaly patterns observed in past El Niño events.

4. ENSO diversity

Spatial distribution, amplitude and temporal evolution of ENSO differ from event to event. Figure 9 shows diversity of ENSO that are categorized based on SST anomaly patterns in different ENSO events by Capotondi et al. (2015). The 1997/98 El Niño event shown in right panel has peak of SST anomaly in the eastern part of equatorial Pacific, which is a typical pattern of the canonical El Niño. During 2004-05, on the other hand, the positive SST anomalies peak near the date line, with no significant warming in the eastern part of the equatorial Pacific. The several kind of names for this type of El Niño has been used with different definitions. For example, Ashok et al. (2007) named it "El Niño Modoki" and Kao and Yu (2009) named it "Central Pacific (CP) El Niño". The canonical El Niño events mentioned above are often referred as "eastern Pacific (EP) El Niño". Distribution of ENSO events in longitude–amplitude plane (left panel) shows that both warm and cold events occur over a broad zonal range. It is also noticed that the strongest events occur in the eastern Pacific. EP El Niño events generally have larger amplitudes than EP La Niña events. In the central Pacific, on the other hand, CP La Niña events tend to be slightly stronger than CP El Niño events.

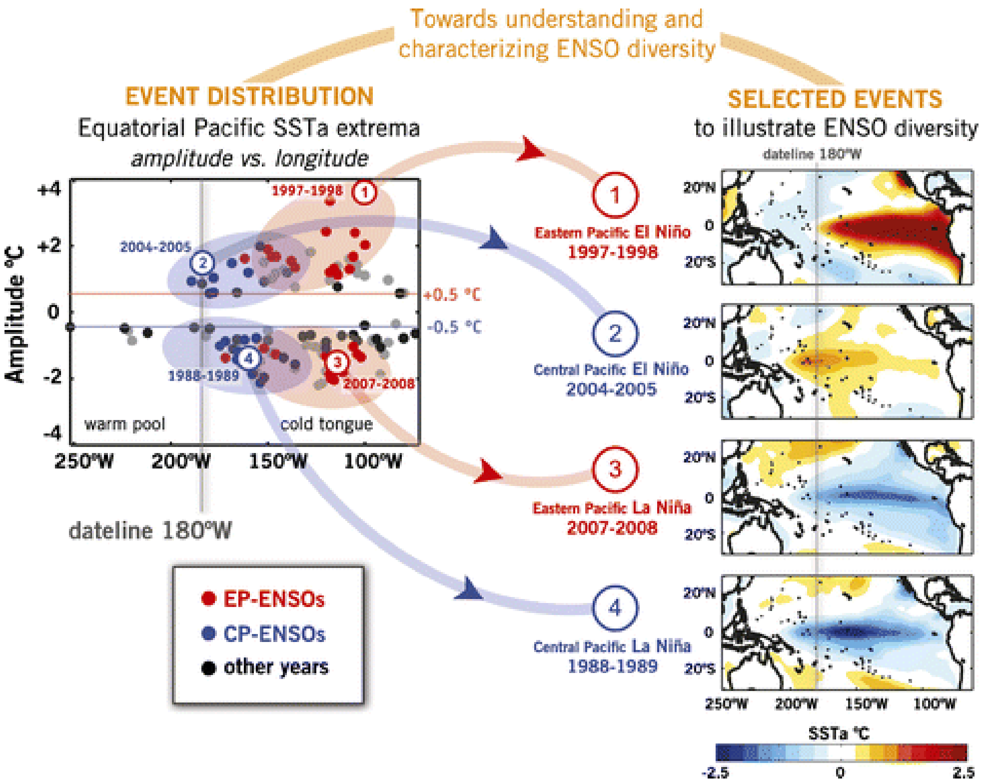

Figure 9 (left) Distribution of boreal winter SST anomaly peaks in the longitude–amplitude plane in the period 1900-2013. Each dot corresponds to the peak value in the region 2°S-2°N, 110°E-90°W. (right) The spatial distributions of SST anomaly for specific warm and cold events of either type. From Capotondi et al. (2015).

5. Interannual variability in the tropical Indian Ocean - IOBW and IOD

Recently, it has been widely known that SST variability in the tropical Indian Ocean has a great influence on the climate variability in the Asian and African regions. There are two major SST modes coupled with atmosphere in the tropical Indian Ocean. One is the Indian Ocean Basin Wide (IOBW) mode that the SST anomalies vary uniformly in the tropical Indian Ocean and another is Indian Ocean Dipole (IOD) mode that SST anomalies indicate zonal dipole structure in the tropical Indian Ocean (Saji et al. 1999).

The IOBW has a close correlation with ENSO (Klein et al. 1999). During an El Niño event, SST anomalies in the tropical Indian Ocean increase and the maximum warming of the Indian Ocean occurs from March to May, lagging the peak of SST anomalies in the eastern equatorial Pacific, i.e., El Niño event by about 3 months (left panel of Figure 10). Typically, warmer SST in the Indian Ocean continues until boreal summer, though El Niño event terminates in boreal spring. This positive SST anomalies in boreal summer influence the tropical atmospheric circulation over the northwestern Pacific in addition to the Indian Ocean (Indian Ocean Capacitor Effect: Xie et al. 2009, right panel of Figure 10).

The positive (negative) IOD is typically characterized by negative (positive) SST anomalies in the eastern (western) part of the equatorial Indian Ocean during boreal summer to autumn (Figure 11). The easterlies anomalies and westward shift of active convection area in the equatorial Indian Ocean associated with those SST anomalies further strengthen the zonal gradient of SST anomalies via Bjerknes feedback. Thus, the positive IOD cause a heavy rainfall over the east Africa and droughts over the Indonesian region (Saji et al., 1999; Saji and Yamagata, 2003).

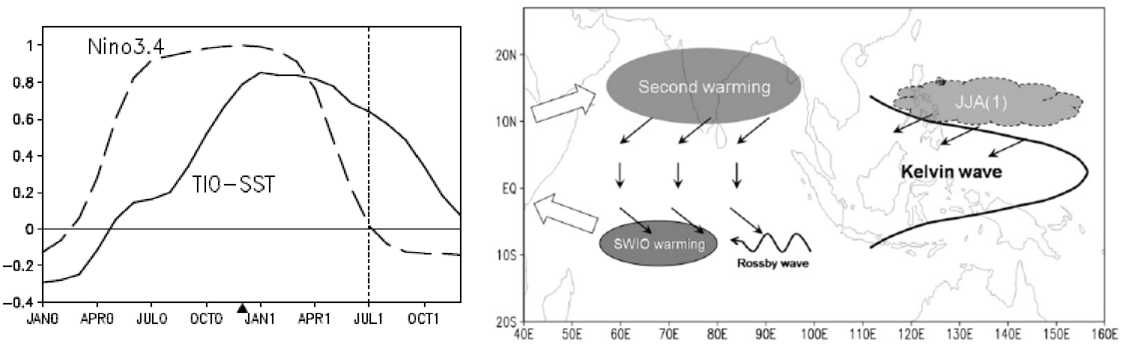

Figure 10 (left) Correlation of tropical Indian Ocean (20°S-20°N, 40°-100°E) SST (solid) with the NIÑO.3.4 (5°S-5°N, 170°-120°W) SST index for November-January. Numerals in parentheses denote years relative to El Niño: 0 for its developing and 1 for decay year. From Xie et al. (2009). (right) Schematic view of El Niño teleconnection into the Indo-NW Pacific. From Xie et al. (2010).

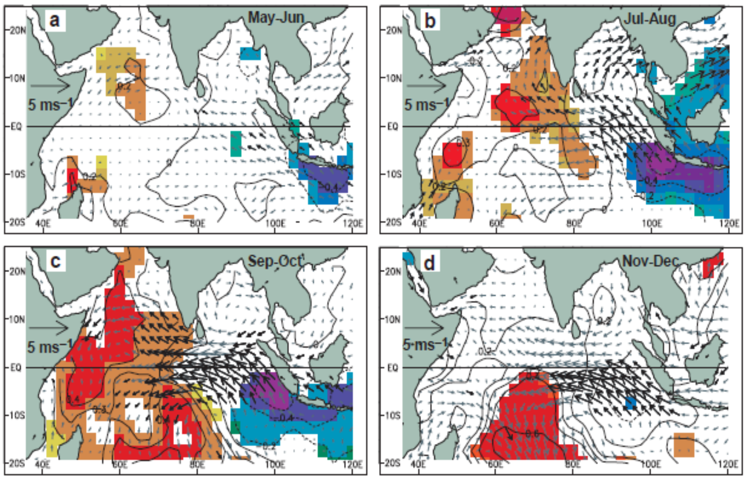

Figure 11 A composite maps of Indian Ocean Dipole (IOD) mode. Evolution of composite SST and surface wind anomalies from May- June (a) to Nov-Dec (d). Anomalies of SSTs and winds exceeding 90% significance are indicated by shading and bold arrows, respectively. From Saji et al. (1999).

References

Ashok, K., S. K. Behera, S. A. Rao, H. Weng, and T. Yamagata, 2007: El Niño Modoki and its possible teleconnections. *J. Geophys. Res.*, 112, C11007, doi:10.1029/2006JC003798.

Bjerknes, J., 1969: Atmospheric teleconnection from the equatorial Pacific. *Mon. Wea. Rev.*, 97, 163-172.

Capotondi, A. et al., 2015: Understanding ENSO Diversity. *Bull. Amer. Meteor. Soc.*, 96, 921-938, doi: 10.1175/BAMS-D-13-00117.1.

Easterling, D. R., and M. F. Wehner, 2009: Is the climate warming or cooling? *Geophys. Res. Rett.*, 36, L08706.

Jin, F.-F., 1997a: An equatorial ocean recharge paradigm for ENSO. Part I: Conceptual model. *J. Atmos. Sci.*, 54, 811-829.

Jin, F.-F., 1997b: An equatorial ocean recharge paradigm for ENSO. Part II: A stripped-down coupled model. *J. Atmos. Sci.*, 54, 830-847.

Kao, H. Y., and J. Y. Yu, 2009: Contrasting eastern Pacific and central Pacific types of ENSO. *J. Climate*, 22, 615-632, doi:10.1175/2008JCLI2309.1.

Klein, S. A., B. J. Soden, and N. C. Lau, 1999: Remote sea surface temperature variations during ENSO: Evidence for a tropical atmospheric bridge. *J. Climate*, 12, 917-932.

Mantua, N. J., S. R. Hare, Y. Zhang, J. M. Wallace, and R. C. Francis, 1997: A Pacific interdecadal climate oscillation with impacts on salmon production. *Bull. Amer. Meteor. Soc.*, 78, 1069-1079.

Meinen, C. S., and M. J. McPhaden, 2000: Observations of warm water volume changes in the equatorial Pacific and their relationship to El Niño and La Niña. *J. Climate*, 13, 3551-3559.

Philander, S. G. H., 1990: *El Niño, La Niña, and the Southern Oscillation*. Academic Press, 289pp.

Saji, N. H., B. N. Goswami, P. N. Vinayachandran, and T. Yamagata, 1999: A dipole mode in the tropical Indian Ocean. *Nature,* 401, 360-363.

Saji, N. H., and T. Yamagata, 2003: Possible impacts of Indian Ocean Dipole mode events on global climate. *Clim. Res.*, 25, 151-169, 2003.

Schopf, P. S., and M. J. Suarez, 1988: Vacillations in a coupled ocean-atmosphere model. *J. Atmos. Sci.*, 45, 549-567.

Suarez, M. J., and Schopf, P. S., 1988: A delayed action oscillator for ENSO. *J. Atmos. Sci.*, 45, 3283-3287.

Xie, S.-P., K. M. Hu, J. Hafner, H. Tokinaga, Y. Du, G. Huang, and T. Sampe, 2009: Indian Ocean capacitor effect on Indo-western Pacific climate during the summer following El Niño. *J. Climate*, 22, 730-747.

Xie, S.-P. Y. Du, G. Huang, X.-T. Zheng, H. Tokinaga, K. Hu, and Q. Liu, 2010: Decadal shift in El Niño influences on Indo-western Pacific and East Asian climate in the 1970s. *J. Climate*, 23, 3352-3368.

Yasuda, T., 2016: Interannual to decadal variability in the tropical oceans. *TCC Training Seminar Textbook, 17-26*

Wang, C., and J. Picaut, 2004: *Understanding ENSO physics - A review*, in Earth's Climate: The Ocean-Atmosphere Interaction, Geophysical Monograph Series, Volume 147, edited by C. Wang, S.-P. Xie, and J. A. Carton, pp. 21-48, AGU, Washington, D. C., 2004.

JMA's Ensemble Prediction System (EPS) for Seasonal Forecasting

JMA's Ensemble Prediction System (EPS) for Seasonal Forecasting

1. Numerical Prediction

Figure 1 shows a simplified conceptual chart of "Numerical Prediction". A numerical model is made from many kinds of physical laws and a large number of grids. If you input an initial atmospheric condition and boundary conditions to a numerical model, you can get to know a future atmospheric condition as an output.

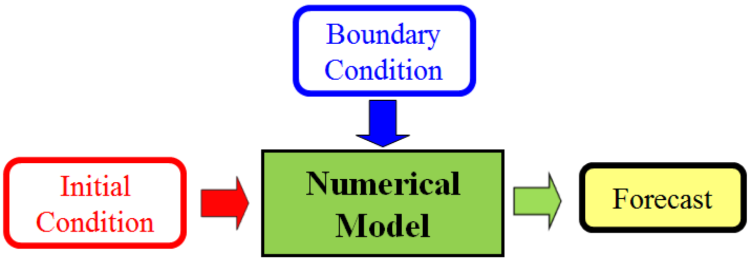

Figure 1 Conceptual Chart of Numerical Prediction

In this case, boundary conditions mean many kinds of seasonal variable natural factors except for atmosphere such as sea surface temperatures (SSTs), sea ices and snow covers. In general, variations of boundary conditions are much slower than a variation of atmosphere.

2. Predictability

Figure 2 shows a simplified conceptual chart of "Predictability". There are mainly 2 types of predictabilities. "Predictability of 1st kind" depends on an initial atmospheric condition. A variation of atmosphere is so fast that information of an initial atmospheric condition is lost rapidly. On the other hand, "Predictability of 2nd kind" depends on boundary conditions. Because variations of boundary conditions are slow, they make a long-range forecast possible.

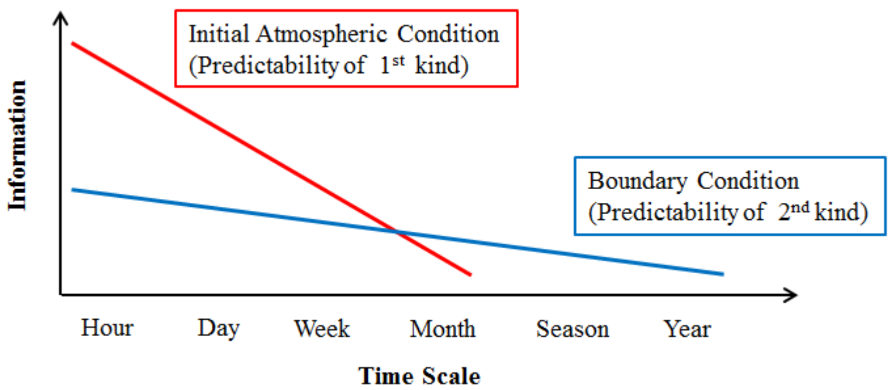

Figure 2 Conceptual Chart of Predictability

By the way, atmospheric phenomena have their own temporal and spatial scales (Figure 3). Long-range forecasts for short-life and small-scale phenomena such as tornadoes and cyclones are impossible, because they are sensitive to an initial atmospheric condition. Conversely, long-range forecasts for long-life and large-scale phenomena such as seasonal oscillations and monsoons are possible, because they are sensitive to boundary conditions rather than an initial atmospheric condition.

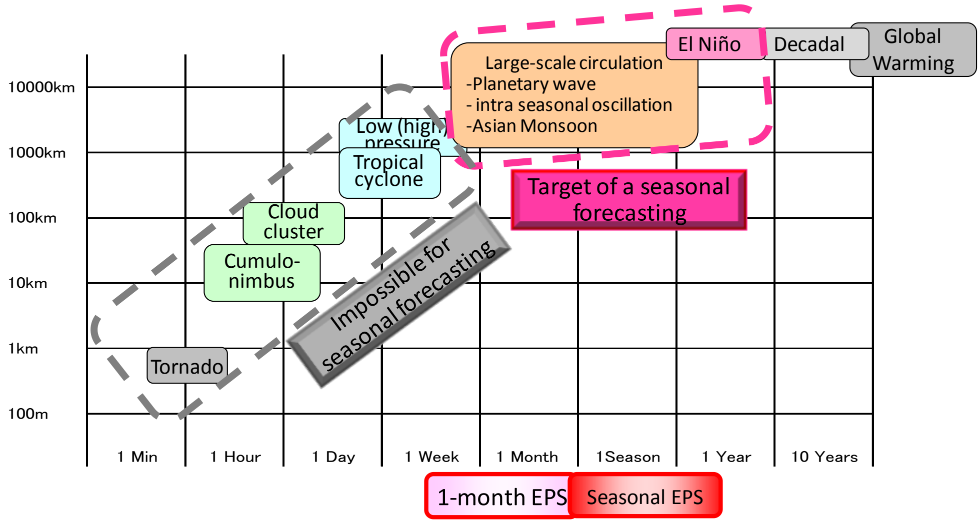

Figure 3 Temporal and Spatial Scale of Atmospheric Phenomena

3. Uncertainty and Ensemble Prediction

Because atmosphere has chaotic nature, a small error in an initial condition grows rapidly. However, it is impossible to know a perfect initial condition even with the use of high precise observations. Therefore, it is essential to consider <u>uncertainty</u> when forecasting. Ensemble prediction makes it possible to estimate uncertainty caused by initial condition errors with similar calculations from a little bit different multiple initial conditions. The individual calculation is called "Ensemble member" and the standard deviation among all members is called "Ensemble spread" (Figure 4).

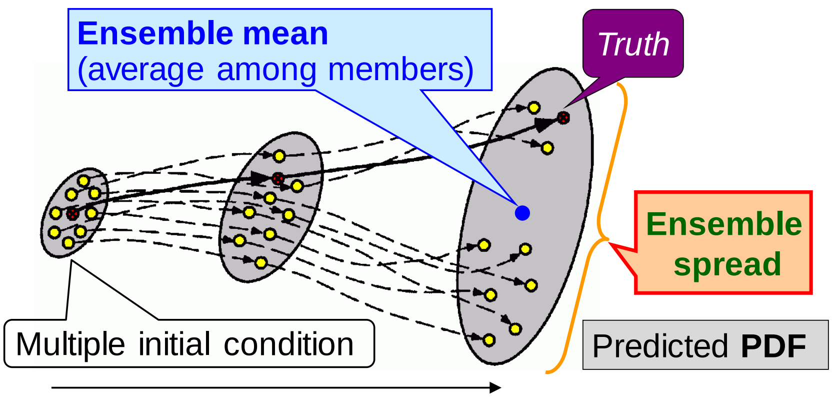

Figure 4 Conceptual Chart of Ensemble Prediction

In order to efficiently represent initial observational errors with initial perturbations (multiple initial conditions), the Breeding of Growing Mode (BGM) and Singular Vector (SV) methods are used. The BGM method finds out the perturbation grew before the initial time with a forecast and assimilation cycle (Figure 5). This method is simple but necessary to keep a forecast and assimilation cycle even for the time except the initial time.

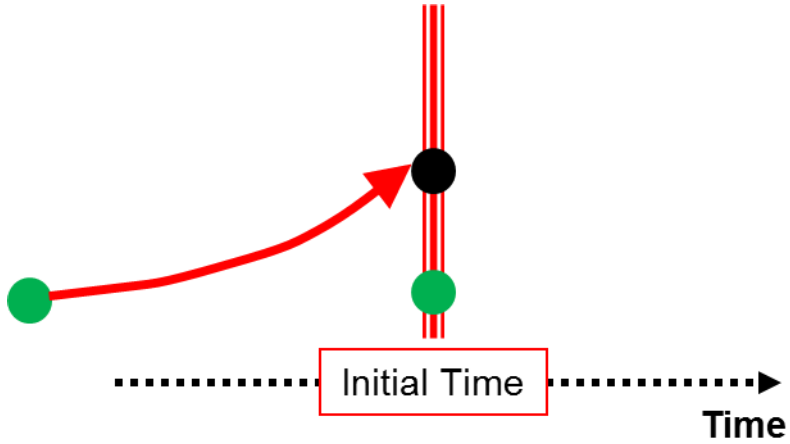

Figure 5 Conceptual Chart of the Breeding of Growing Mode method

On the other hand, the SV method finds out the fastest growing perturbation after the initial time with the use of a tangent linear model which is obtained by locally linearizing the original nonlinear NWP model and its adjoint model (Figure 6). The SV method can find better perturbations, but requires heavier resources for calculation and development.

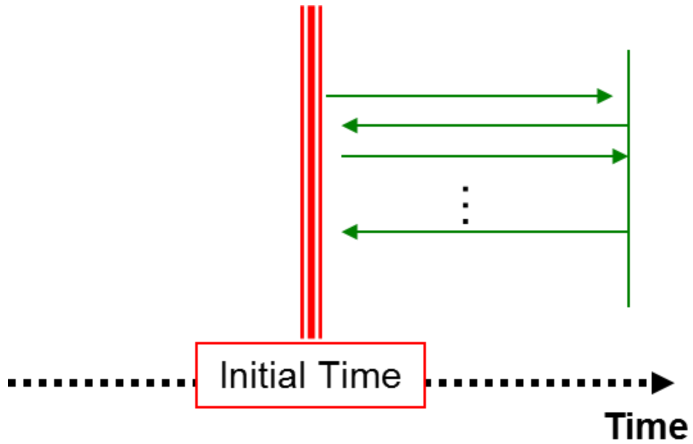

Figure 6 Conceptual Chart of the Singular Vector method

Lagged Average Forecasting (LAF) is one of the ensemble prediction techniques. LAF ensemble prediction is calculated with the combination of ensemble predictions not only from latest initial condition but also from older initial conditions (Figure 7). LAF is an easy method for ensemble prediction and make it possible to share computer resources between some days. It is also possible to get a significant ensemble spread even at initial time. However, the prediction skill from older initial conditions is generally worse than that from latest initial condition.

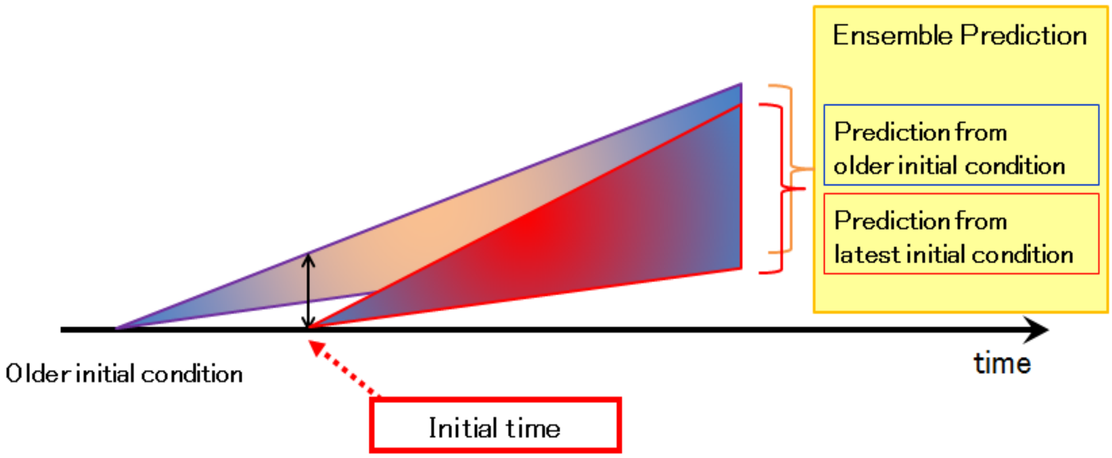

Figure 7 Conceptual Chart of Lagged Average Forecasting (LAF)

Actually uncertainty is caused by imperfection not only of initial conditions but also of numerical prediction models. In order to consider uncertainty caused by imperfection of numerical prediction models, multi-model ensemble (MME) system and stochastic physics scheme are often used. MME is an EPS using some different numerical ensemble prediction models and stochastic physics scheme is a calculation method which controls some parameterization of physical calculations with random numbers (Figure 8).

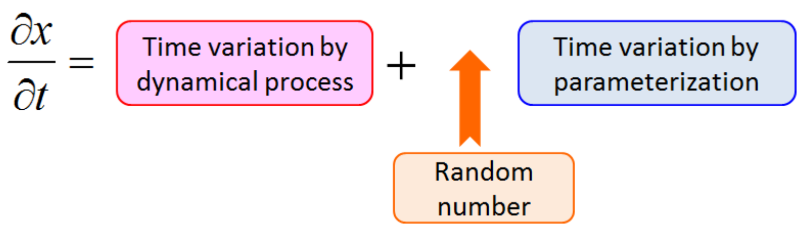

Figure 8 Conceptual Chart of Stochastic Physics Scheme

4. WMO Forecast Classification

In line with "WMO's Manual on the Global Data-Processing and Forecasting System"[1], forecasts are classified by their ranges as Table 1. Seasonal forecasting, which is the main topic of the TCC seminar, corresponds to extended- and long-range forecasting (shaded in table 1).

Table 1 Definitions of meteorological forecasting range classified by WMO

	Forecasting target period
Nowcasting	Up to 2 hours
Very short-range weather forecasting	Up to 12 hours
Short-range forecasting	Beyond 12 hours and up to 72 hours
Medium-range weather forecasting	Beyond 72 hours and up to 240 hours
Extended-range weather forecasting	Beyond 10 days and up to 30 days
Long-range forecasting	Beyond 30 days up to two years
Climate forecasting	Beyond two years

5. JMA's Global and Seasonal Ensemble Prediction System

JMA uses a high-resolution atmospheric general circulation model (AGCM) named "Global Ensemble Prediction System (EPS)" for extended-range weather forecast, because predictability of 1st kind is important. JMA also uses a coupled ocean-atmosphere general circulation model (CGCM) named "Seasonal Ensemble Prediction System (EPS)" for long-range forecast, because predictability of 2nd kind is important. The specifications of these two EPSs are listed as table 2. Actually, the model resolution for Seasonal EPS is lower than that for Global EPS, because CGCM requires more computer resources than AGCM due to calculation not only of atmospheric component but also of oceanic component. In order to make initial perturbations, Global EPS uses the combination of SV, LAF and LETKF[2] methods, while Seasonal EPS uses the combination of BGM and LAF methods. The both models also adopt a stochastic physics scheme to consider uncertainty caused by model's imperfection. The last major upgrades are March 2017 for Global EPS and June 2015 for Seasonal EPS. JMA normally upgrades Global EPS every few years and Seasonal EPS about every half decade.

If you need more detailed information, see the "Numerical Weather Prediction of JMA" website (http://www.jma.go.jp/jma/jma-eng/jma-center/nwp/nwp-top.htm).

1 http://www.wmo.int/pages/prog/www/DPS/Publications/WMO_485_Vol_I.pdf
2 LETKF is a Local Ensemble Transform Kalman Filter based on Hunt et al. (2007).

Table 2 Specification of the One-month and Seasonal EPS (as of January 2018)

	Global EPS	Seasonal EPS
Upgrade	Last: March 2017 Frequency: Every few years	Last: June 2015 Frequency: About every half decade
Model	AGCM (Atmospheric General Circulation Model)	CGCM (Coupled Ocean-atmosphere General Circulation Model)
Resolution	Horizontal: 40km(TL479) up to 18days 55 km (TL319) after 18 days Vertical: 100 levels up to 0.01 hPa	* Atmospheric component Horizontal: 110 km (TL159) Vertical: 60 levels up to 0.1 hPa * Oceanic component Horizontal: 1.0º longitude, 0.3–0.5º latitude (with Tri-pole grid) Vertical: 52 levels + Bottom Boundary Layer
Forecast range	Up to 34 days	7-month (initial month of Sep., Oct., Feb., Mar., Apr) 4 months (the other initial month)
Oceanic conditions	Prescribed SST perturbation Prescribed Sea Ice distribution	MRI.COM (Oceanic General Circulation Model) Interactive Sea Ice Model
Green House Gases	Constant	RCP4.5 scenario for 6 GHGs
Ensemble methods	Singular Vector (SV), Lagged Average Forecast (LAF), Local Ensemble Transform Kalman Filter (LETKF), Stochastic physics scheme	Breeding of Growing Modes (BGM), Lagged Average Forecast (LAF), Stochastic physics scheme
Ensemble size	50 (combination of 13-11 SVs & 4 initial LAF at 12 hour interval)	51 (combination of 13-12 BGMs & 4 initial LAF at 5-day interval)
Frequency of operation	Every Tuesday and Wednesday	Every 5 days
Frequency of model product creation	Once a week Every Thursday	Once a month Around 20th (no later than 22nd) of every month

6. Hindcast

Hindcasts are systematic forecast experiments for past cases. Hindcast experiments are performed usingthe operational model. Hindcast datasets are used not only to estimate the systematic biases and prediction skills but also to develop statistical models. In order to calculate a large number of past events, huge computer resources are required. However, because of the limited computer resources, ensemble size and calculation frequency for hindcasts are less than those for operational forecasts. The detailed differences between hindcasts and operational forecasts are listed as table 3. For the initial date on which no hindcast was performed, virtual hindcast data is created with a linear interpolation method using before and after initial dates on which hindcasts were performed.

Table 3 Differences between hindcasts and operational forecasts

* Global EPS

	Hindcast	Operational system
Initial Condition	JRA-55	Global Analysis (Newer System than JRA-55)
Ensemble size	5 (5 SVs, not using LAF and LETKF)	50 (13-11 BGMs & 4 initial LAF with 12 hour interval)
Forecast range	Initial date + 40 days	2, 3, 4,...31, 32 days from the latest initial date (Wednesday)
Initial date	10th, 20th, end of month	00UTC and 12UTC on every Tuesday and Wednesday
Target period for hindcast	Available : 1981.1-2017.3 Verification: 1981.1-2010.12	–

* Seasonal EPS

	Hindcast	Operational system
Initial Condition	JRA-55	JRA-55
Ensemble size	5 (5 BGM)	51 (13-12 BGMs & 4 days LAF with 5-day interval)
Forecast range	Lead time from 0 to 6 months as shown in the correspondence table below	(4-month EPS) Lead time from 1 to 3 as shown in the correspondence table below (7-month EPS) DJF (initial month of Sep., Oct.) JJA (initial months of Feb., Mar. and Apr.)
Initial date	24 initial dates a year (16th Jan., 31th Jan., 10th Feb., 25th Feb., ,... 12th Dec. and 27th Dec.)	Once a month
Target period for hindcast	Available : 1979-2014 Verification: 1981-2010	–

Correspondance between lead times (months) and initial dates

Target Month Initial Date	Jan.	Feb.	Mar.	Apr.	May	Jun.	Jul.	Aug.	Sep.	Oct.	Nov.	Dec.
27-Dec, 12-Dec	0	1	2	3	4	5	6					
31-Jan, 16-Jan		0	1	2	3	4	5	6				
25-Feb, 10-Feb			0	1	2	3	4	5	6			
27-Mar, 12-Mar				0	1	2	3	4	5	6		
26-Apr, 11-Apr					0	1	2	3	4	5	6	
31-May, 16-May						0	1	2	3	4	5	6
30-Jun, 15-Jun	6						0	1	2	3	4	5
30-Jul, 15-Jul	5	6						0	1	2	3	4
29-Aug, 14-Aug	4	5	6						0	1	2	3
28-Sep, 13-Sep	3	4	5	6						0	1	2
28-Oct, 13-Oct	2	3	4	5	6						0	1
27-Nov, 12-Nov	1	2	3	4	5	6						0

7. Prediction Skills

7.1. Global EPS

The score graphs for operational one month forecasts (Figure 9) show upward trends, reflecting historical model improvements. However, temporary increases and decreases are sometimes seen, corresponding to major and unsettled ENSO events respectively. Compering between the stable period in early 2000s and that in early 2010s, anomaly correlation of geo-potential height at 500hPa (Z500) for 28-day mean forecast in the Northern Hemisphere has been improved about 1.2 points.

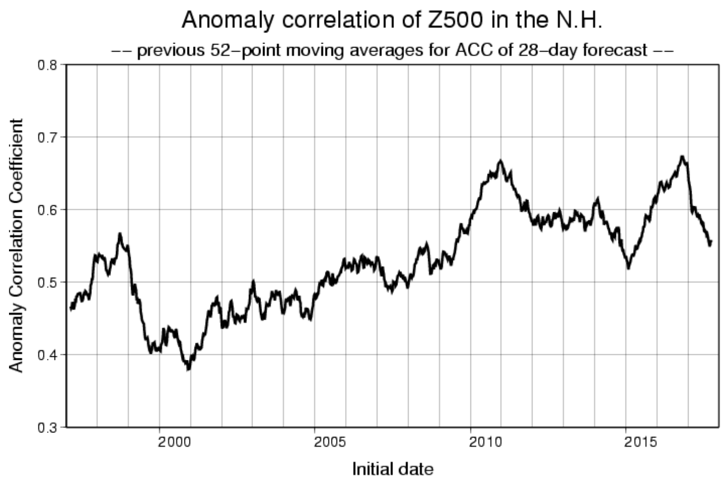

Figure 9 Anomaly correlation of geopotential height at 500hPa for operational 28 day mean forecasts in the Northern Hemisphere

Focusing on the area-averaged daily rainfall scores in summer monsoon season, onset and offset seasons are somehow predictable but mature season is difficult to predict (Figure 10). It is assumed that seasonal oscillations such as Madden Julian Oscillation (MJO) and Boreal Summer Inter Seasonal Oscillation (BSISO) make monsoon rainfall forecast difficult. According to the hindcast verification, MJO is somehow predictable up to around 25 days, but velocity and amplitude biases are seen.

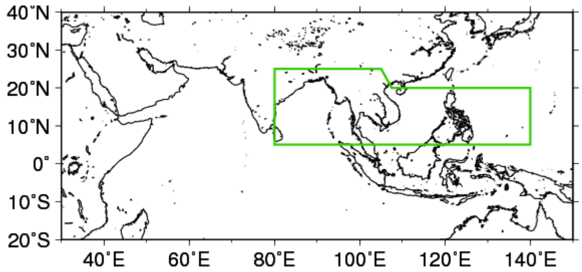

Initial month	Daily Rainfall Correlation (28day mean)
May	0.46
June	0.09
July	0.38
August	0.30

Figure 10 Region (left) and score (right) of a daily monsoon rainfall index for hindcast

7.2. Seasonal EPS

Figure 11 shows the prediction skill diagrams for SST indexes. Prediction skills for NINO.3 (i.e., El Niño/La Niña) have large seasonal differences. According to hindcast verification, prediction skills through boreal spring season are generally low and called “Spring Barrier”. Prediction skills for NINO.WEST, IOBW and Dipole Mode Index (DMI) also have large seasonal differences. Prediction skills for NINO.WEST are low for the forecast during tropical cyclone season and those for IOBW are low for the forecast through summer monsoon season. Those for DMI are predictable only for the target in autumn season.

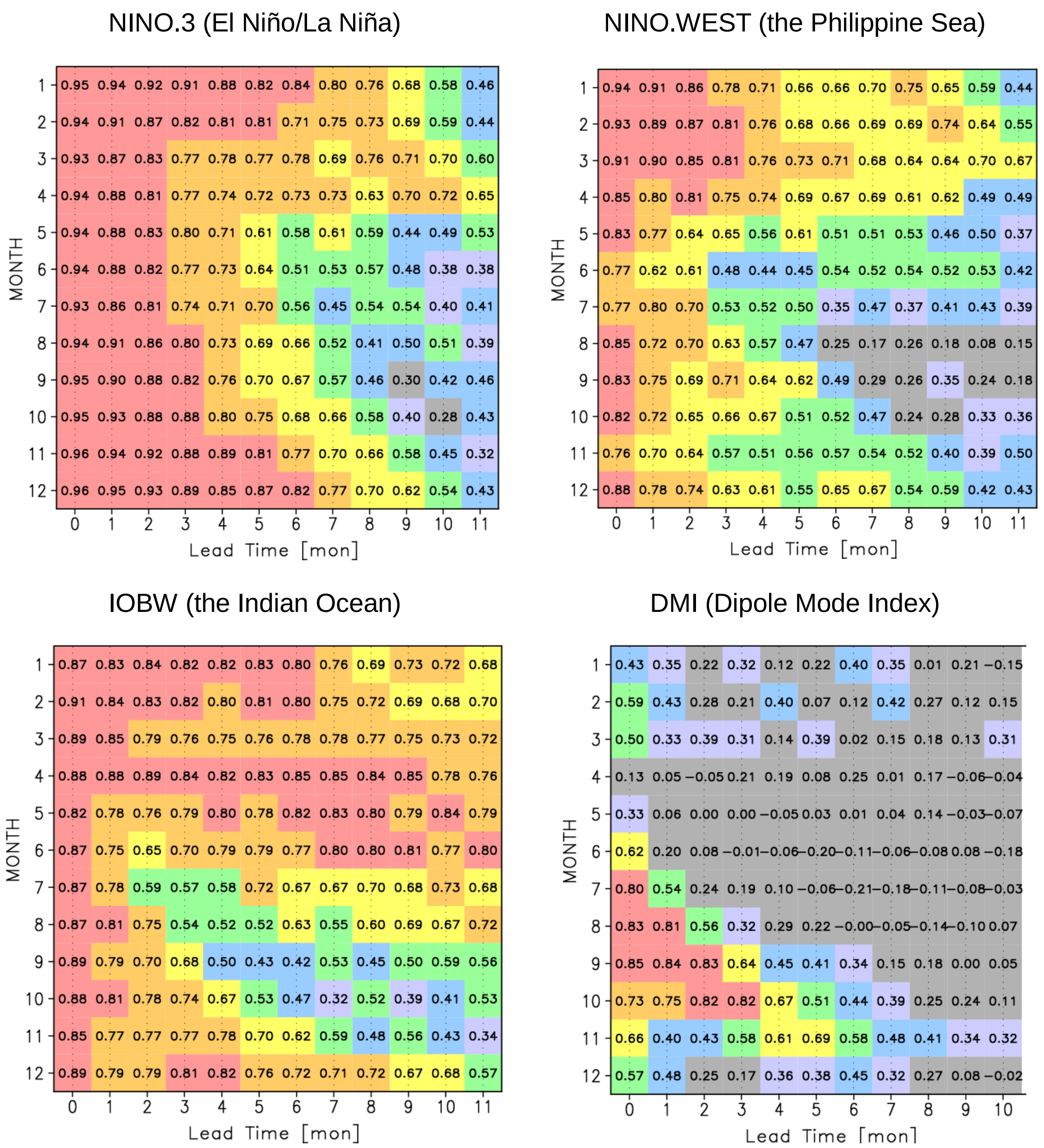

Figure 11 Prediction skill diagram of SST index

Although seasonal EPS considers variabilities of sea ices and 6 kinds of greenhouse gases, 2m temperature trends have serious bias in some regions (Figure 12). Especially, resent cooling trends in and around Siberia and the Bering Sea during boreal winter are not seen in the hindcast results. Because forecast scores of hindcast for 2m temperature is also low in and around Siberia and the Bering Sea during boreal winter, 2m temperature forecasts should be interpret with caution in those regions.

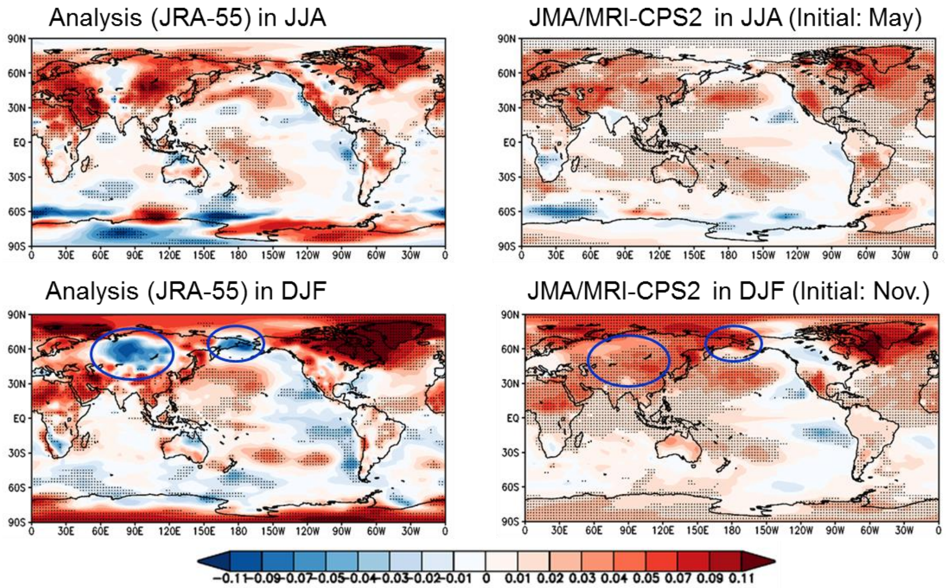

Figure 12 Comparison between analysis and hindcast of 2m temperature trends

Focusing on the area-averaged monthly rainfall scores in summer monsoon season, onset and offset seasons are somehow predictable but mature season is difficult as well as Global EPS (Figure 13). It is assumed that seasonal oscillations such as Madden Julian Oscillation (MJO) and Boreal Summer Inter Seasonal Oscillation (BSISO) make monsoon rainfall forecast difficult. However, according to hindcast verification, the MJO forecast skill is better than Global EPS especially for the amplitude.

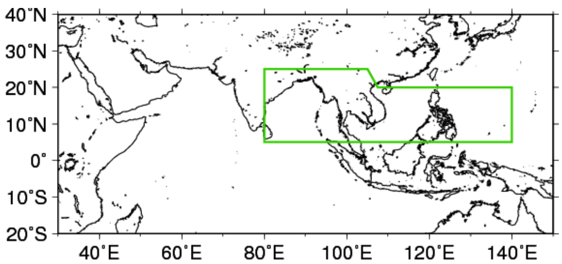

Target Month	LAF period	
	11/26 April	16/31 May
June	0.20	0.63
July	0.08	0.21
August	0.05	-0.07
Sept.	0.45	0.30

Figure 13 Region (left) and score (right) of a monsoon index for hindcast

8. Products

8.1. TCC Website for Numerical Model Prediction (GPC Tokyo)

Many kinds of numerical prediction model products are available on the TCC website (Figure 14). The some products such as extreme weather prediction and gridded data require authentication. These products are displayed for reference by National Meteorological and Hydrological Services (NMHSs) and not forecast for any nation.

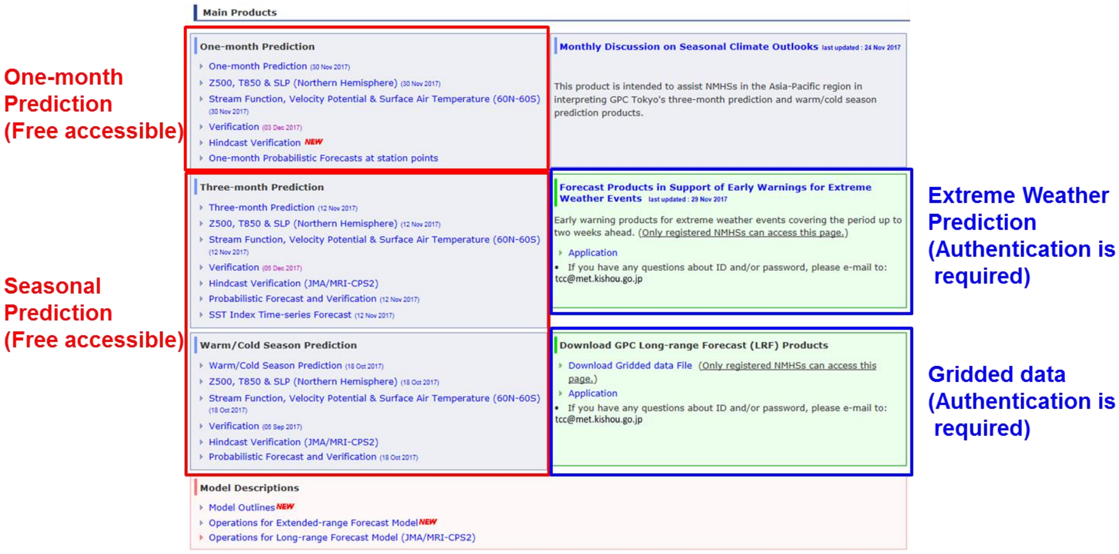

Figure 14 TCC's numerical weather prediction (GPC Tokyo) website
http://ds.data.jma.go.jp/tcc/tcc/products/model/index.html

(a) One-month Prediction Products

- Forecast maps
- Real-time and hindcast verification charts
- Probabilistic forecasts at station points in Southeast Asia.
- Extreme forecast index (authentication is required)
- Forecast map animation (authentication and high speed internet access are required)
- Gridded data of operational forecasts and hindcasts (authentication is required)

(b) Three month and Warm/Cold Season Products

- Forecast maps
- SST index time-series forecast (available since June 2015)
- Real-time and hindcast verification charts
- Probabilistic forecasts
- Gridded data of operational forecasts and hindcasts (authentication is required)

8.2. Forecast Maps

Various kinds of forecast maps are available on the numerical model prediction website of TCC. The period for forecast maps are 1st week, 2nd week, 3-4 week and 28 days average for one month prediction and 1-month and 3-month average for seasonal prediction. The elements are as follows.

(a) Tropical Maps (60S-60N)

- Daily mean precipitation (RAIN)
- Velocity Potential (CHI200)
- Stream Function at 200hPa (PSI200)
- Stream Function at 850hPa (PSI850)
- Geo-potential height at 500hPa (Z500)
- Sea Level Pressure (PSEA)
- Surface Temperature (TS)
- Sea Surface Temperature (SST)
- Stream Function and wind at 850hPa (only for seasonal EPS)

(b) Northern Hemisphere Maps

- Geo-potential height at 500hPa (Z500)
- Temperature at 850hPa (T850)
- Sea Level Pressure (PSEA)

SST, RAIN and CHI200 maps are useful to understand tropical convections. PSI200, PSI850 and wind at 850hPa maps are useful to understand Rossby and Kelvin responses (i.e., Matsuno-Gill responses) associated with tropical convections. Meanwhile, Z500 map is useful to understand teleconnection patterns such as Pacific North America (PNA), Tropical Northern Hemisphere (TNH), Eurasia (EU) and West Pacific (WP) patterns. In general, predictabilities over mid- and high- latitudes are small but those for phenomena associated with topical convections are relatively high, because tropical convections are well influenced by slow variable SSTs. Also, PSEA map is useful to understand Arctic Oscillation (AO), North Atlantic Oscillation (NAO) and the strength of North Pacific High, Siberian High, Aleutian Low and so on. In addition, model output temperature maps are necessary to check statistical guidance reliability. If predicted temperatures in guidance are different from those in model, you should investigate the cause.

8.3. Verification Scores and Maps

Various kinds of verification products are available on the numerical model prediction website of TCC. The elements are as follows.

(a) Verification products for Global EPS operational forecast

- Error maps for every forecast
- Historical and Recent scores
- Reliability diagrams for each season
- ROC curves for each season

(b) Verification products for Global EPS hindcast

- Bias maps
- Hindcast maps
- Time-series Circulation Index
- Verification Score Maps

(c) Verification products for Seasonal EPS operational forecast

- Error maps for every forecast

(d) Verification Products for Seasonal EPS hindcast

- Deterministic score Maps
- Probabilistic score Diagrams
- Probabilistic score Maps
- Time-series Circulation Index
- ENSO Index score
- ENSO Index time-series
- Hindcast Maps

Error maps and the operational scores are useful to understand the real-time operational model performance. Hindcast score maps are useful to understand the spatial distribution of model prediction skills. In the low prediction skill region, it is not recommended to use model output directly. Statistical relationships to the high skill region and calibration using past observation should be considered. Time-series circulation indexes for hindcast are useful to understand model predictabilities of various kinds of focal phenomena such as El Niño/La Niña, Indian Ocean Dipole (IOD), monsoon rainfalls and circulations. Higher skill phenomena should be used for explanation of forecast reasons.

8.4. Probabilistic forecast

JMA provides calibrated tercile probabilistic forecasts for 3-monthand warm and cold season averaged sea surface temperature, surface temperature and precipitation over the global based on the seasonal EPS (Figure 15). An ordered probit model is used to calibrate tercile probabilistic forecasts using 30-year hindcasts (1981-2010). The thresholds of tercile are determined so that the climatological chance of occurrence for each category is 33.3 % for the hindcast period from 1981 to 2010.

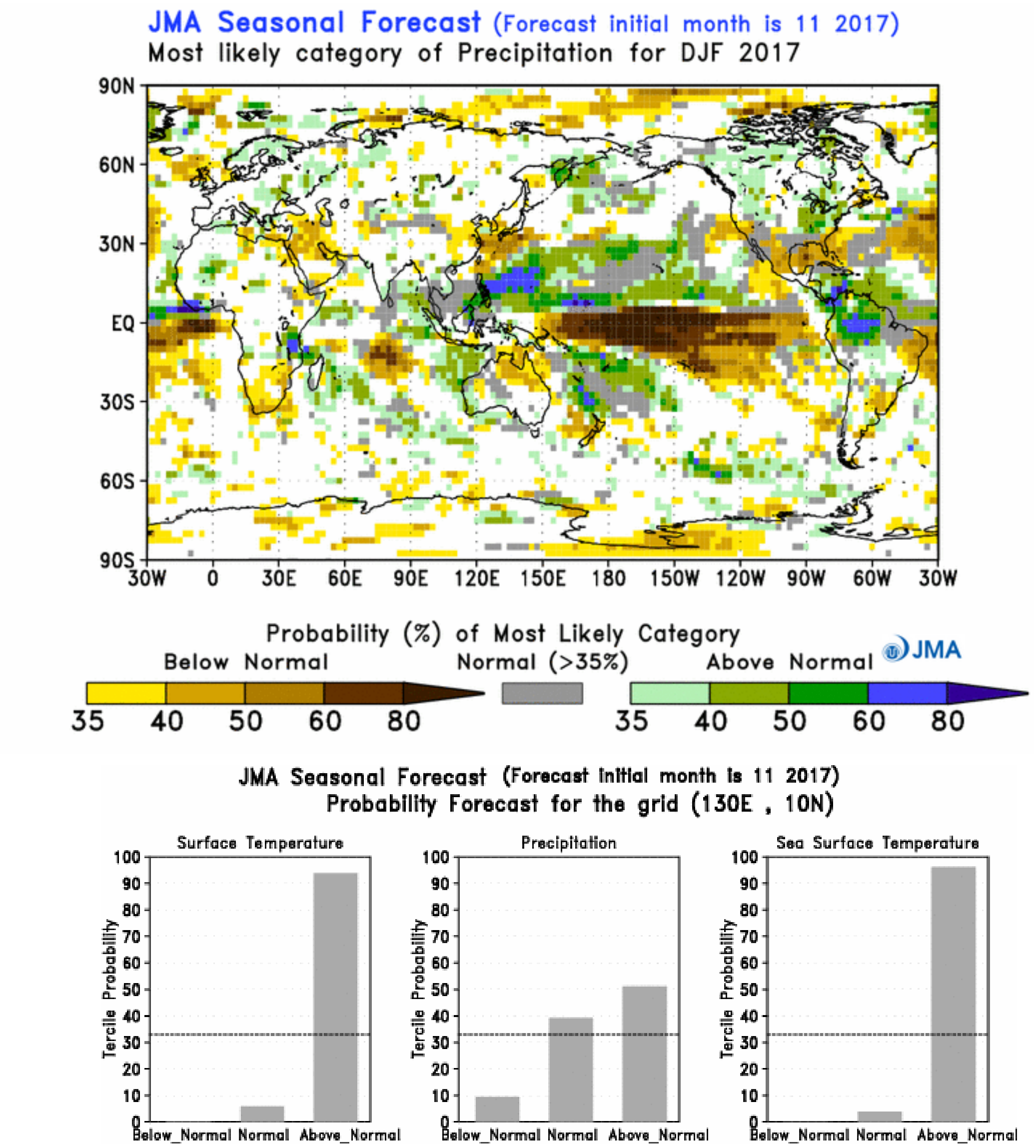

Figure 15 Probabilistic forecast map (top) and tercile probability of a point (bottom)

http://ds.data.jma.go.jp/tcc/tcc/products/model/probfcst/3-mon/index.html

http://ds.data.jma.go.jp/tcc/tcc/products/model/probfcst/warm_cold_season/index.html